JAEA-Technology
2020-012
DOI:10.11484/jaea-technology-2020-012

Practical Guide on Soil Sampling, Treatment, and Carbon Isotope Analysis for Carbon Cycle Studies

Jun KOARASHI, Mariko ATARASHI-ANDOH, Hirohiko NAGANO
Untung SUGIHARTO, Chakrit SAENGKORAKOT, Takashi SUZUKI
Yoko SAITO-KOKUBU, Natsuko FUJITA, Naoki KINOSHITA
Haruyasu NAGAI, Naishen LIANG, Hiroyuki MATSUZAKI
and Genki KATATA

Environment and Radiation Sciences Division
Nuclear Science and Engineering Center
Nuclear Science Research Institute
Sector of Nuclear Science Research

October 2020
Japan Atomic Energy Agency
日本原子力研究開発機構

JAEA-Technology

本レポートは国立研究開発法人日本原子力研究開発機構が不定期に発行する成果報告書です。
本レポートの入手並びに著作権利用に関するお問い合わせは、下記あてにお問い合わせ下さい。
なお、本レポートの全文は日本原子力研究開発機構ホームページ（https://www.jaea.go.jp）
より発信されています。

国立研究開発法人日本原子力研究開発機構 研究連携成果展開部 研究成果管理課
〒319-1195 茨城県那珂郡東海村大字白方 2 番地4
電話 029-282-6387, Fax 029-282-5920, E-mail:ird-support@jaea.go.jp

This report is issued irregularly by Japan Atomic Energy Agency.
Inquiries about availability and/or copyright of this report should be addressed to
Institutional Repository Section,
Intellectual Resources Management and R&D Collaboration Department,
Japan Atomic Energy Agency.
2-4 Shirakata, Tokai-mura, Naka-gun, Ibaraki-ken 319-1195 Japan
Tel +81-29-282-6387, Fax +81-29-282-5920, E-mail:ird-support@jaea.go.jp

JAEA-Technology 2020-012

Practical Guide on Soil Sampling, Treatment, and Carbon Isotope Analysis for Carbon Cycle Studies

Jun KOARASHI, Mariko ATARASHI-ANDOH, Hirohiko NAGANO[*1], Untung SUGIHARTO[*2], Chakrit SAENGKORAKOT[*3], Takashi SUZUKI, Yoko SAITO-KOKUBU[+1], Natsuko FUJITA[+1], Naoki KINOSHITA[+2], Haruyasu NAGAI, Naishen LIANG[*4], Hiroyuki MATSUZAKI[*5] and Genki KATATA[*6]

Environment and Radiation Sciences Division,
Nuclear Science and Engineering Center, Nuclear Science Research Institute,
Sector of Nuclear Science Research
Japan Atomic Energy Agency
Tokai-mura, Naka-gun, Ibaraki-ken

(Received July 30, 2020)

There is growing concern that recent rapid changes in climate and environment could have a significant influence on carbon cycling in terrestrial ecosystems (especially forest ecosystems) and could consequently lead to a positive feedback for global warming. The magnitude and timing of this feedback remain highly uncertain largely due to a lack of quantitative understanding of the dynamics of organic carbon stored in soils and its responses to changes in climate and environment. The tracing of radiocarbon (natural and bomb-derived ^{14}C) and stable carbon (^{13}C) isotopes through terrestrial ecosystems can be a powerful tool for studying soil organic carbon (SOC) dynamics. The primary aim of this guide is to promote the use of isotope-based approaches to improve our understanding of the carbon cycling in soils, particularly in the Asian region.

The guide covers practical methods of soil sampling; treatment and fractionation of soil samples; preparation of soil samples for ^{13}C (and stable nitrogen isotope, ^{15}N) and ^{14}C analyses; and ^{13}C, ^{15}N, and ^{14}C measurements by the use of isotope ratio mass spectrometry and accelerator mass spectrometry (AMS). The guide briefly introduces ways to report ^{14}C data, which are frequently used for soil carbon cycling studies. The guide also reports results of a case study conducted in a Japanese forest ecosystem, as a practical application of the use of isotope-based approaches. This guide is mainly intended for researchers who are interested but are not experienced in this research field. The guide will hopefully encourage readers to participate in soil carbon cycling studies, including field works, laboratory experiments, isotope analyses, and discussions with great interest.

Keywords: Radiocarbon (^{14}C), Stable Carbon and Nitrogen Isotopes (^{13}C and ^{15}N), Global Carbon Cycle, Soil, Forest Ecosystem, Sampling, Accelerator Mass Spectrometry (AMS)

This guide was prepared through the project “Research on Climate Change using Nuclear and Isotopic Techniques” organized by the Ministry of Education, Culture, Sports, Science and Technology, Japan (MEXT), under the framework of the Forum for Nuclear Cooperation in Asia (FNCA).

+1 Tono Geoscience Center
+2 Aomori Research and Development Center
*1 Post-Doctoral Fellow until March 2020
*2 National Nuclear Energy Agency of Indonesia
*3 Thailand Institute of Nuclear Technology
*4 National Institute for Environmental Studies
*5 The University of Tokyo
*6 Ibaraki University

JAEA-Technology 2020-012

炭素循環研究のための土壌採取、処理、炭素同位体分析の実践ガイド

日本原子力研究開発機構
原子力科学研究部門　原子力科学研究所　原子力基礎工学研究センター
環境・放射線科学ディビジョン

小嵐 淳、安藤 麻里子、永野 博彦[*1]、Untung SUGIHARTO[*2]、Chakrit SAENGKORAKOT[*3]、
鈴木 崇史、國分(齋藤) 陽子[+1]、藤田 奈津子[+1]、木下 尚喜[+2]、永井 晴康、
梁 乃申[*4]、松崎 浩之[*5]、堅田 元喜[*6]

（2020 年 7 月 30 日受理）

近年急速に進行する温暖化をはじめとした地球環境の変化は、陸域生態系（とりわけ森林生態系）における炭素循環に変化をもたらし、その結果、温暖化や環境変化の進行に拍車をかける悪循環が懸念されている。しかしながら、その影響の予測には大きな不確実性が伴っており、その主たる要因は、土壌に貯留する有機炭素の動態とその環境変化に対する応答についての定量的な理解の不足にある。放射性炭素（^{14}C）や安定炭素（^{13}C）同位体の陸域生態系における動きを追跡することは、土壌有機炭素の動態を解明するうえで有力な研究手段となりうる。本ガイドは、同位体を利用した土壌炭素循環に関する研究を、特にアジア地域において促進させることを目的としたものである。

本ガイドは、土壌の採取、土壌試料の処理、土壌有機炭素の分画、^{13}C の同位体比質量分析法による測定及びその試料調製、ならびに ^{14}C の加速器質量分析法による測定及びその試料調製に関する実践的手法を網羅している。本ガイドでは、炭素循環研究において広く用いられる ^{14}C 分析結果の報告方法についても簡単に紹介する。さらに、同位体を利用した研究手法の実際的応用として、日本の森林生態系において実施した事例研究の結果についても報告する。本ガイドによって、同位体を利用した炭素循環研究に興味を持って参画する研究者が増加し、地球環境の変化の仕組みについての理解が大きく進展することを期待する。

このガイドは、アジア原子力協力フォーラムの枠組みを活用して文部科学省が主催する「気候変動科学プロジェクト」における研究活動の一環として作成されたものである。

原子力科学研究所：〒319-1195 茨城県那珂郡東海村大字白方 2 番地 4
+1 東濃地科学センター
+2 青森研究開発センター
*1 2020 年 3 月まで博士研究員
*2 National Nuclear Energy Agency of Indonesia
*3 Thailand Institute of Nuclear Technology
*4 国立環境研究所
*5 東京大学
*6 茨城大学

Contents

目　次

1. Introduction

The world's soils store more than twice the amount of carbon (C) present in the atmosphere. They produce the dominant emission flux of C to the atmosphere through microbial decomposition of soil organic carbon (SOC), which currently balances the net flux of C entering terrestrial ecosystems through photosynthesis in plants (i.e., the difference between the influx of C by photosynthesis and the outflux of C by plant respiration, **Fig. 1.1**)[1,2]. The gross C fluxes through microbial decomposition of SOC are estimated to be about 10 times that of the C emission flux due to the use of fossil fuels[2]. Hence, even a small change in the dynamics (stock and turnover) of SOC could have a significant impact on the atmospheric CO_2 concentration, the global C cycle, and consequently the Earth's climate system[3,4].

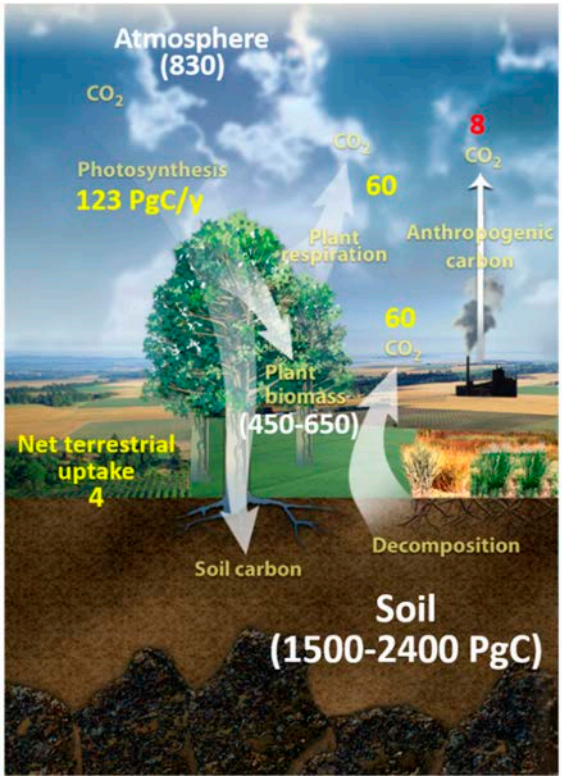

Fig. 1.1. Simplified schematic of the terrestrial carbon cycle.
White numbers indicate reservoir mass (i.e., carbon stocks in PgC) and yellow numbers indicate annual carbon fluxes (in PgC y^{-1}). Diagram is from U.S. Department of Energy, Office of Science. Data are from IPCC[1,2].

There are a number of natural and artificial processes that can potentially affect the SOC dynamics. Increase in soil temperature due to global warming can accelerate microbial decomposition of SOC and enhance the release of CO_2 from soil to the atmosphere[5–8]. This could cause positive feedback that

further accelerates global warming. Studies using coupled carbon cycle–climate models suggest that this feedback could lead to a doubling of the projected warming by the end of this century[9,10]. Soil moisture is also known as a major factor controlling SOC decomposition[11,12]. Fluctuations of soil water content in the Asian monsoon region have reportedly been increasing since the 20th century. This is owing to the decreased frequency and increased year-by-year variation of precipitation, accompanied by the progression of climate change[13]. Recent studies indicate that repeated dry–wet cycles of soils can enhance the microbial decomposition of SOC through alteration in substrates available for soil microorganisms[14–16]. Land-use change is one of the most important artificial processes to change the stock and turnover of SOC. Significant losses of SOC have been observed following the conversion of forests to agricultural land in many regions over the world[17]. Management practices, such as thinning, clear-cutting, and planting for forests[18] and tilling and plowing for agricultural land[19] can also affect the SOC dynamics.

The tracing of radiocarbon (^{14}C) through terrestrial ecosystems is a powerful tool for quantitatively understanding SOC dynamics on two different time scales: centuries to millennia, and years to decades[4,20,21]. Natural ^{14}C is produced at a relatively constant rate in the upper atmosphere by cosmic ray interactions. Therefore, ^{14}C content in SOC can be a useful indicator of how long SOC has resided in the soil on a time scale of centuries to millennia, because it decreases with time as a result of the radioactive decay of ^{14}C (with a physical half-life of 5730 years) after the addition of ^{14}C as organic C into the soil. Atmospheric weapons testing in the 1950s and early 1960s injected a large amount of "bomb-^{14}C" into the atmosphere with a peak value in 1964 that almost doubled the natural ^{14}C concentration[22]. Since the nuclear test ban treaty, the amount of ^{14}C in atmospheric CO_2 has gradually decreased as the bomb-^{14}C has moved into the ocean and terrestrial C reservoirs (and as the atmospheric CO_2 concentration has become diluted by the burning of ^{14}C-free fossil fuels). This global bomb-^{14}C spike has proven to be useful as a tracer for studying SOC dynamics on a time scale of years to decades, because it enables us to evaluate how much organic carbon recently fixed via photosynthesis has incorporated into SOC in the soil[3,4,20,23–26].

Recent developments of the ^{14}C measurement techniques by the use of accelerator mass spectrometry (AMS) have opened a new range of possible uses of ^{14}C because of their analytical capability for a small quantity of sample, and thus have great potential to facilitate studies to constrain the complicated dynamics of SOC. The availability and quality of ^{14}C measurements have recently been increasing, and as we know well, ^{14}C measurements have been vigorously carried out for the purpose of ^{14}C dating (i.e., age determination), which contribute to the progress of a diverse range of research fields such as archaeology and geology[27,28]. Radiocarbon has also proven very useful in SOC dynamics studies; however, applications of ^{14}C to these studies are still limited, and therefore currently no satisfactory and standard approach to quantifying SOC dynamics is established[29–31].

This guide aims at introducing ways to study SOC dynamics using ^{14}C (and stable carbon and nitrogen isotopes) and describing its practical procedures including: soil sampling, treatment, and carbon isotope analysis. The guide also reports results of a case study conducted in a Japanese forest ecosystem, as a practical application of the use of isotope-based approaches. This guide is mainly intended for researchers who are interested but, inexperienced in the field of climate change science and in the applications of nuclear and isotope techniques. We hope this guide will contribute to a rapid expansion of the application of ^{14}C to studying SOC dynamics, particularly in Asian countries, and as a result, contribute to an improved understanding of the SOC dynamics and its interactions with climate and environmental changes in these regions.

2. Soil Sampling

The objective of soil sampling is to collect samples that will best represent the average physicochemical properties (including organic carbon content) of an investigated site. To achieve this, an undisturbed area should be selected. Avoid heavily populated areas. In general, soils, forest soils in particular, have spatial variability. These variabilities are caused by multiple factors, such as bedrock type and parent material, climate, vegetation, disturbances, and their combined effects. One must take into consideration all these sources of spatial variability to systematically collect soil samples and describe soil properties at the site. This is why sampling strategies and methodologies must be selected with care.

There are two widely used methods for soil sampling: (1) the pit-digging method and (2) the core-sampling method. Each of the methods have their advantages and disadvantages. Therefore, a choice of the soil sampling method depends on the purpose of the study and precision required.

2.1. Pit-digging Method

In the pit-digging method, a soil pit is dug, and soil samples are collected from a face of the soil pit at an arbitrary interval of soil depth (**Fig. 2.1**). Use a spade to dig a large rectangular hole (soil pit), about 60 cm deep (in the case of collecting soil samples down to the depth of 50 cm, for example) and an area of 100 cm × 100 cm. Please note that the area where soil samples are collected should be undisturbed during the digging.

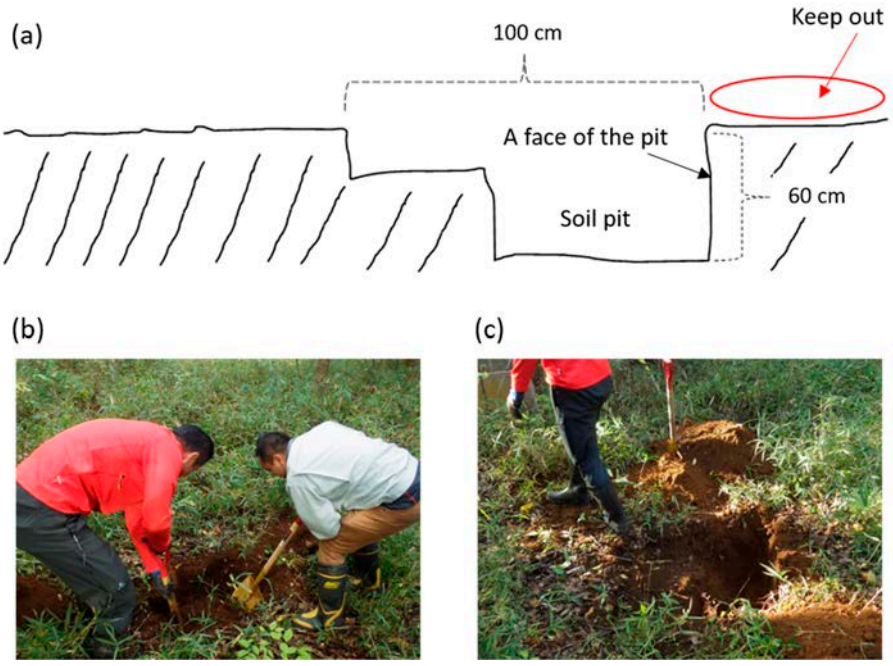

Fig. 2.1. Schematic diagram (a) and photos (b, c) of a soil pit prepared for soil sampling.

Soil samples are then collected layer by layer from a face of the pit as shown in **Fig. 2.2**. In forest soils, mineral soil is generally covered by forest-floor organic (litter) layers. Therefore, the litter layers are first removed completely, and then the soil samples are collected. **Fig. 2.2** shows the case of soil sampling of 10-cm interval layers up to a total of 50 cm. Soil samples are collected using a hand shovel and clean trays. Place the tray at the bottom of the target layer, and slide down the face of each layer from top to bottom using shovel, after removing a thin surface of the face of the soil for avoiding contamination with soils that were tumbled down from upper soil layers[25,32]. The tools should always be kept clean by wiping, for example with paper towels, to avoid cross-contamination of soil samples with samples of different soil layers. If the litter layer is also a research target, it should be collected from a defined area (e.g., 30 cm × 30 cm, this is to determine the amount of litter materials per unit area) and kept as a sample[33]. The samples collected are put into plastic bags.

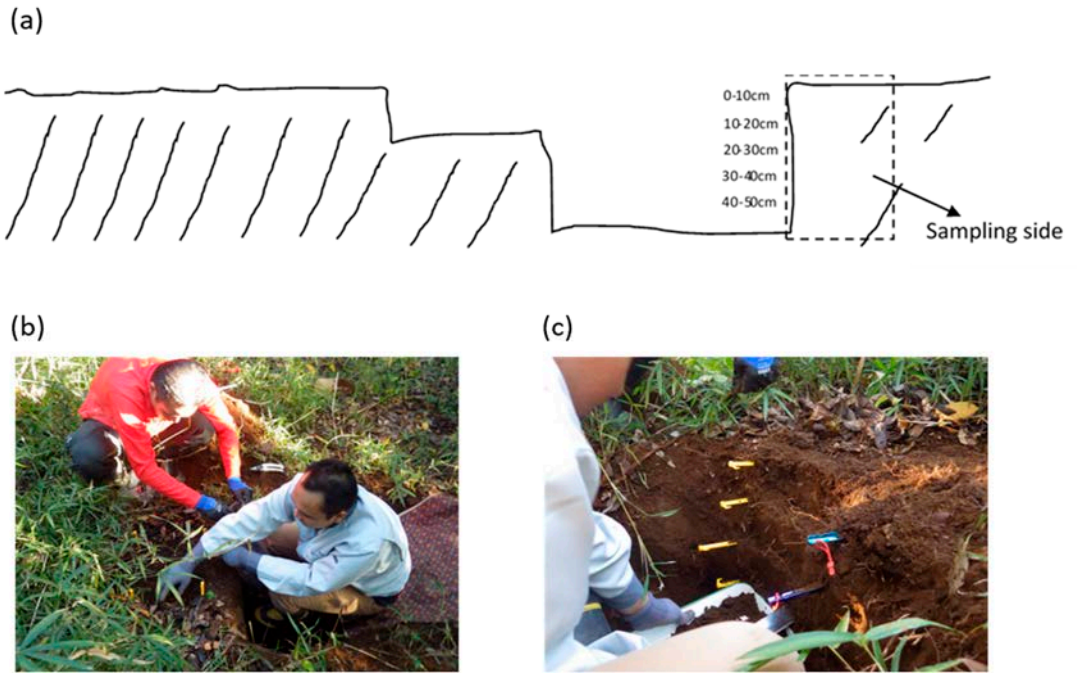

Fig. 2.2. Schematic diagram (a) and photos of soil sampling: collection of litter samples from forest-floor organic layer (b) and collection of soil samples at the depth interval of 10 cm (c).

In the pit-digging method, soil samples are collected from an arbitrary volume by grab sampling, and the bulk density of the soil cannot be determined. Therefore, we need to collect soil samples separately for the purpose of determining the bulk density (**Fig. 2.3**). Bulk density is a measure of how dense and tightly packed a sample of soil is, which is necessary to evaluate the inventory of soil organic carbon in the soil (see Section 3.3 for details). Bulk density is determined by measuring the mass of dry soil per

unit of volume (e.g., in g cm^{-3}). The bulk density of soil depends not only on the soil type but also the depth of soil even in a single soil profile. Soils dominated by minerals have a different bulk density from those rich in organic materials.

A known-volume (100 cm^3) soil sampler is often used to collect soil samples for bulk density determination (**Fig. 2.3**). The following is the operation procedure of soil sampling utilizing a soil sampler Model DIK-1601 (Daiki Rika Kogyo Co., Ltd., Japan): (1) Unscrew the lock pin to open the sampler window; (2) Load the sample cylinder (100 cm^3 in volume) into the sampler and screw the lock pin back on; (3) Push the sampler into the soil until the ground surface reaches the level with the top of the cylinder; (4) Pull the sampler out of the soil and unscrew the lock pin to open the window sampler; (5) Cleanly cut the soil sample at the bottom of the cylinder with a cutter to separate the cylinder from the sampler; (6) Carefully pull the cylinder out of the sampler vertically; (7) Clean soil from the top of cylinder using trowel until the surface reaches the level with the top of the cylinder; and (8) Recover the soil samples from the cylinder and put into a plastic bag.

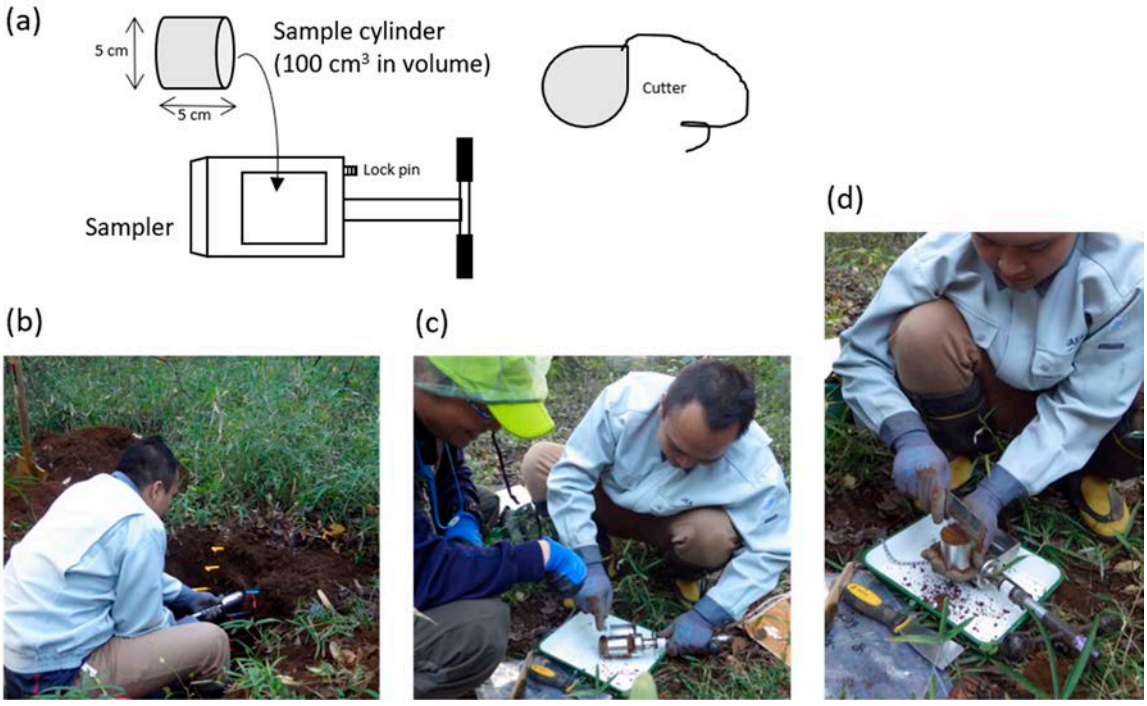

Fig. 2.3. Schematic diagram of a soil sampler for bulk density determination (a) and photos of soil sampling: sampling (b) and sample recovery (c, d).

2.2. Core-sampling Method

A core sampler is used to collect soil samples in this method (**Fig. 2.4**)[4,33,34]. As in the pit-digging method, forest-floor organic (litter) layers are removed (if sites are in forests). Then, the core sampler is placed on the ground surface and driven into the soil approximately 25 cm in depth (in the case of a core sampler with 10-cm diameter and 30-cm long: Model HS-25, Fujiwara Scientific Company, Japan). Before pulling the core sampler out of the soil, it is better to check, by opening the lid of the core sampler, whether the level of soil surface in the area isolated by the core sampler is almost the same as that in the surrounding area. This is to ensure that a significant compaction of soil-core sample does not occur during the sampling. Afterwards, slowly pull the core sampler up and take the plastic bag previously set inside the sampler, which now contains a soil core sample.

Fig. 2.4. Schematic diagram of a soil core sampler (a) and photos of soil core sampling: sampling (b,c) and sample recovery (d).

2.3. Advantages and Disadvantages of the Different Methods

Sampling of forest-floor litter layers varies among soil scientists and, also, on the purpose of the research; therefore, there are no accepted standards for how horizons should be sampled.

The advantages of the core-sampling method are efficiency and practicality. A corrugated knife equipped on the outside edge of the core-sampling frame will generally cut through surface soil layers with no difficulty, even if vegetation has spread large amount of fine roots in the soil. Therefore, once the sample is cut on all sides, it is easy to partition it from the soil. This method provides us with a hopefully undamaged soil core retrieved from a precisely identified location with minimizing contamination of each layer in the soil profile. More importantly, this method enables us to collect soil samples at a very thin depth interval as needed (see Section 3.2); this can sometimes be an essential factor to achieve your research goal[4]. The main disadvantage of this method may be related to the representativeness of the core sample. The area of the core sample collected is normally very small compared with the site-scale target area to be investigated. To overcome this issue, one may collect three or more replicated core samples within the target area to consider the spatial variability of soil samples[33,34]. Another disadvantage may be the relatively high cost of the equipment.

The advantages of the pit-digging method don't require any specific equipment (you only need spade, hand shovel, tray, knife, ruler, plastic bags, skewers, and so on) and can cover a large area. This method is also convenient if you want to obtain large amounts of soil samples from each of the soil layers. However, the strongest advantage of this method is that it enables us to collect soil samples from deeper layers compared with the core-sampling method; this can also sometimes be the key requirement for your research objectives[25]. The disadvantage of this method may be that soil sample in a target soil layer can easily be contaminated with other layers of the soil profile during sampling; therefore, careful sampling procedure is required[32]. This may also be noted as a disadvantage, digging soil pits are labor-intensive.

3. Soil Sample Treatment

Pretreatment is generally required for soil and litter samples prior to soil carbon analysis. It includes drying and sieving of soil samples, both of which are also essential for evaluating SOC stock in the soil. In this chapter, practical methods for pretreatment of soil and litter samples are briefly described. You can find more detailed procedures for soil sample handling and storage[35,36] and for soil physicochemical, mineralogical, and microbiological analyses[37–41] in well-established protocol guides.

3.1. Drying Soil Samples

Soil samples are dried immediately at room temperature (or 50°C in an oven) in a laboratory. If this is not possible then, the samples should be stored in a freezer (at −30°C, for example) to prevent decomposition of organic materials in the samples. Measuring the weight of the soil sample before and after drying allows us to determine the water content of the soil.

3.2. Cutting Soil Core Samples

According to the research purpose, the soil core samples (e.g., 20 cm long) can be divided into several sections (thin-layered samples) in terms of the depth intervals (e.g., 0–2 cm, 2–4 cm, 4–6 cm, …15–20 cm) before drying (**Fig. 3.1a-c**). The core cutting should be conducted for core samples that are in a frozen state by using a saw. This will enable us to precisely obtain thin-layered samples without any cross-contamination[4,33]. An important point that should be kept in mind is that, before cutting each of the thin-layered samples, an outer part of the soil core is peeled away, and only the inner part of the soil core should be used for analysis. This procedure is done to eliminate any possible contamination from the upper to lower soil layers during the sampling[42]. Please note that the weight of the outer part of the soil core should also be measured and considered in the calculation of soil bulk density.

Soil bulk density of each of the separated layers can be estimated as the dry weight of the soil samples (including both inner and outer parts) divided by the volume of the layer (i.e., the cross-section area of the core sample multiplied by the thickness of the layer).

3.3. Sieving Soil Samples

The dried soil samples are sieved through a 2-mm mesh to remove gravel and roots (**Fig. 3.1d**). This procedure is required not only to obtain a homogenized soil sample for analysis, but also to quantify the carbon stock in the soil layer. Weigh both fractions (i.e., > 2 mm and < 2 mm fractions) to calculate the gravel (> 2 mm in size) content in the soil sample. SOC stock in a given soil layer, I_S (kgC m^{-2}), can be calculated as:

$$I_S = BD \cdot C_S \cdot d \cdot (1-g) \qquad \text{(Eq. 3.1)}$$

where BD is the bulk density (kg m^{-3}), C_S is the carbon content of the soil (< 2 mm) sample (kgC kg^{-1} soil), d is the thickness of the layer (m), and g is the gravel content (kg kg^{-1})[25].

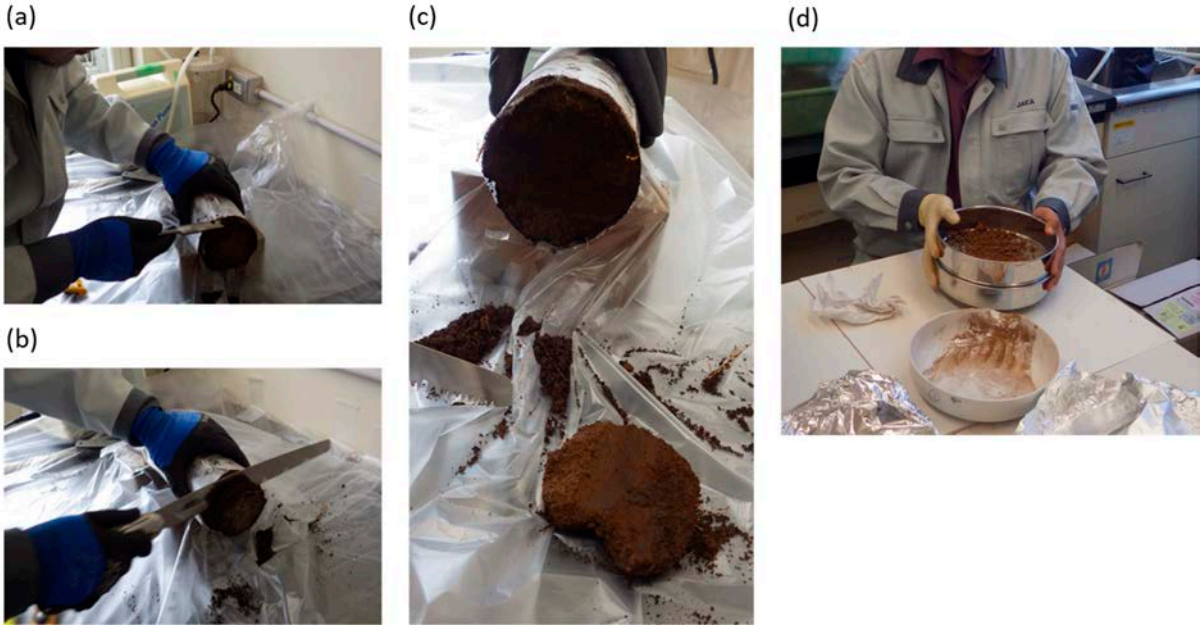

Fig. 3.1. Photos of soil-core cutting (peeling an outer part of the soil core (a), cutting (b), and a thin-layered sample obtained (c)) and sieving of a dried soil sample (d).

3.4. Removing Carbonate Minerals (Inorganic Carbon) from Alkaline Soils

Alkaline soils with high pH values (pH > 7) may contain various soluble carbonate minerals such as sodium bicarbonate and carbonate. These inorganic compounds should be removed before analysis, if the focus of the research is on organic carbon in soils. Treatment of soil samples with hydrochloric acid (HCl) solution can remove such inorganic compounds from the samples because HCl reacts with carbonate to release C as CO_2.

3.5. Treatment for Litter Samples

A different procedure is required for the treatment of litter samples collected from forest-floor litter layers. To obtain a homogenized sample for analysis, litter samples are pulverized by using a blender after removing roots, branches, and stones (**Fig. 3.2**). SOC stock in the litter layer, I_L (kgC m^{-2}), can be calculated as:

$$I_L = C_L \cdot M_L \qquad \text{(Eq. 3.2)}$$

where C_L is the carbon content of the litter sample (kgC kg^{-1}) and M_L is the amount of litter materials per unit area (kg m^{-2}) in the litter layer.

Fig. 3.2. Photos of the treatment for litter samples: separation of a litter sample into leaf-litter fraction and the other (roots, branches, and stones) fraction (a); pulverization of the leaf-litter fraction (b); and homogenized leaf-litter sample (c).

4. Fractionation of Soil Samples

Soil organic carbon (SOC) is a complex mixture of organic compounds with heterogeneous physical, chemical, and biological properties, from undecomposed and partially decomposed plant materials to substances synthesized by soil microbes[43]. SOC also consists of various functional pools that are stabilized by physical and chemical mechanisms in soil[44]. These SOC compounds and pools greatly differ in degradability, and the overall dynamics (stock and turnover) of soil C is thus largely regulated by such a heterogeneous nature of SOC. This demonstrates that SOC modeled as a homogeneous single pool (i.e., only represented as a bulk soil) causes a misunderstanding of the real SOC dynamics. Therefore, quantitative understanding of the heterogeneity in SOC dynamics is a key to accurately predicting the response of soil C to future changes in climate and environment[4].

Fractionation of SOC, as a potentially effective, operational method, has been attempted to separate soil C into SOC fractions with different properties and turnover times[30]. Fractionation methods include: (1) physical separation of SOC into particle- and/or aggregate-size fractions and density fractions[25,45–50]; and (2) chemical extractions to fractionate SOC according to solubility and chemical reactivity[4,25,51–53]. Combinations of some of these physical and chemical fractionation methods have also been proposed[29,30,54]. However, a successful and standard method to identify SOC pools according to turnover time and thus to quantify the SOC dynamics remains unexplored.

The objective of this chapter is to introduce some basic methods for SOC fractionation and to describe practical procedures for the methods.

4.1. Density Fractionation

A density fractionation method is used to separate a soil sample into soil fractions with different densities; this is based on contrasting densities between soil mineral particles (typically 2.5–3.0 g cm^{-3}) and organic materials (< 1.4 g cm^{-3}) in the soil[45,48,55]. Here, as an example, a simple method using a heavy liquid (density of 1.6 cm^{-3}) to separate a soil sample into two fractions: organic matter-dominant low-density fraction (LF, < 1.6 g cm^{-3}) and mineral-dominant high-density fraction (HF, > 1.6 g cm^{-3}), is described. The flowchart of the physical fractionation method is shown in **Fig. 4.1**.

Soil samples (approximately 5 ml, after removing roots by hand) are weighed into 50 ml centrifuge tubes and mixed with 35 ml of 1.6 g cm^{-3} sodium polytungstate (SPT) liquid (**Fig. 4.2**). The tubes are shaken gently and centrifuged at 3000 rpm for 30 min, and the floating materials (LF) are aspirated onto a pre-baked glass microfiber filter (pore size: 0.7 μm). The cycle of gentle shaking, centrifugation, and aspiration is repeated until no LF remained floating (typically three times). The LF is then rinsed at least three times with ultrapure water (a minimum of 45 ml) on the filter under vacuum using a separate collector, and dried at 50°C in an oven[50].

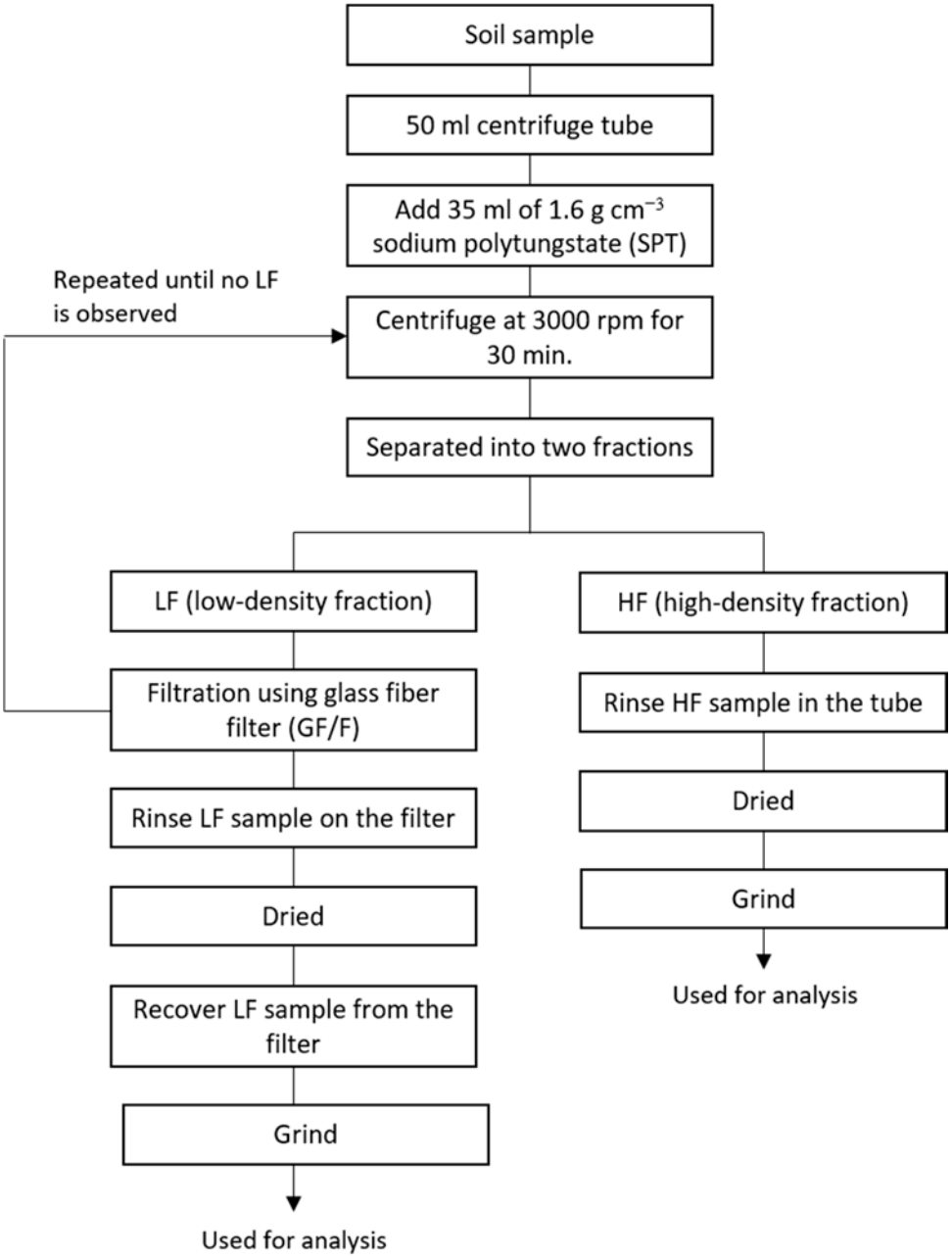

Fig. 4.1. Flowchart of the density fractionation method.

After floating off the LF materials completely, the residue (HF) in the centrifuge tubes is rinsed more than 7 times with ultrapure water (45 ml) by shaking and centrifuging at 3000 rpm for 15 min to remove SPT from the HF samples, and then dried at 50°C in an oven[50)].

Mass balance (the initial weight of the sample vs. the sum of the weights of LF and HF samples) is used to assess the completeness of recovery. Note that dissolved organic carbon lost to SPT solution and

ultrapure water during the fractionation is not recovered; the carbon loss during fractionation may sometimes reach more than 10% of the total soil C for some soils[25,31,55,56]. The fractions obtained are then homogenized by grinding using a mortar and pestle (after removing roots again if necessary), and then are used for analysis.

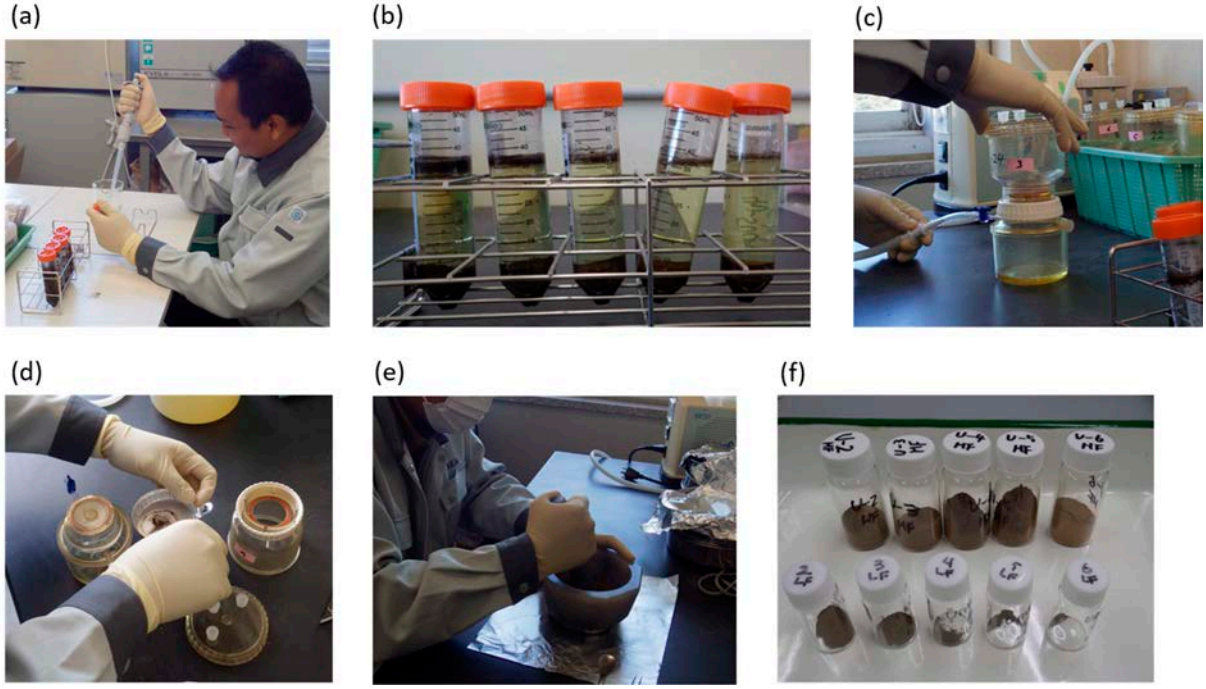

Fig. 4.2. Photos of the physical fractionation procedure: addition of a heavy liquid (SPT) into a centrifuge tube with soil sample (a); separation of soil samples into low-density (LF) and high-density (HF) fractions (b); filtration of LF sample (c); collection of LF sample (d); grinding of HF sample (e); and the obtained LF and HF samples (f).

4.2. Aggregate-size Fractionation

An aggregate-size fractionation method is used to separate a soil sample into soil fractions with different size classes of aggregates in which primary soil particles (clay, silt, and sand) are bound to each other with the help of soil organic matter as binding agent[49,57–59]. Here, as an example, a simple aggregate-size fractionation method to separate a soil sample into two fractions: macroaggregate fraction (> 250 μm in size) and microaggregate fraction (< 250 μm), is described. The flowchart of the aggregate-size fractionation method is shown in **Fig. 4.3**.

Soil sample (approximately 10 g, after removing roots by hand) is put on a polyethylene mesh sheet having 250 μm pores (approximately 30 cm × 30 cm in size, Nichika, Kyoto, Japan) attached to a

sieving set (Mini-sieve, Merck, Germany). Both the mesh sheet and the sieving set should be cleaned with detergent before fractionation. The sieving set is submerged in 200 ml of ultrapure water in a 500-ml beaker for 10 minutes, and is then slowly moved in and out of the water repeatedly for 2 min (approximately 50 times in 5 cm strokes) (**Fig. 4.4**). The particulate materials retained on the mesh sheet are dried at 50 ºC for 24 h, and recovered as macroaggregates (> 250 μm in size). The solution in the beaker is filtrated with a 0.45-μm pore-sized nitrocellulose membrane filter (Merck Millipore, MA, USA) under vacuum condition. The particulate materials retained on the membrane filter are dried at 50ºC for 24 h, and recovered as microaggregates (< 250 μm in size). Each of the aggregate-size fractions is then homogenized by grinding before analysis. Note that, as in the physical fractionation, organic carbon dissolved in ultrapure water (< 0.45 μm) is lost during fractionation, if the dissolved fraction is not recovered.

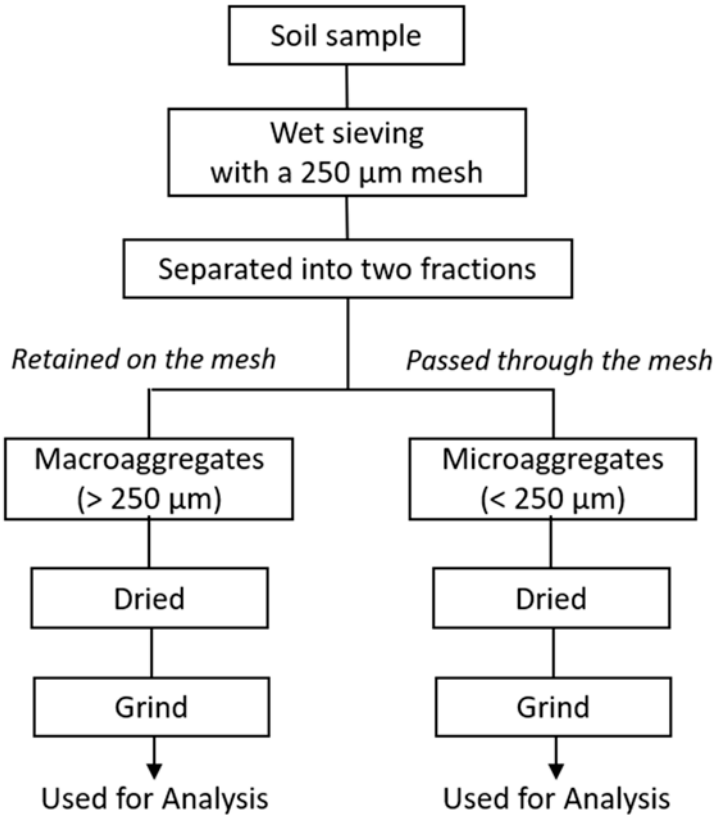

Fig. 4.3. Flowchart of the aggregate-size fractionation method.

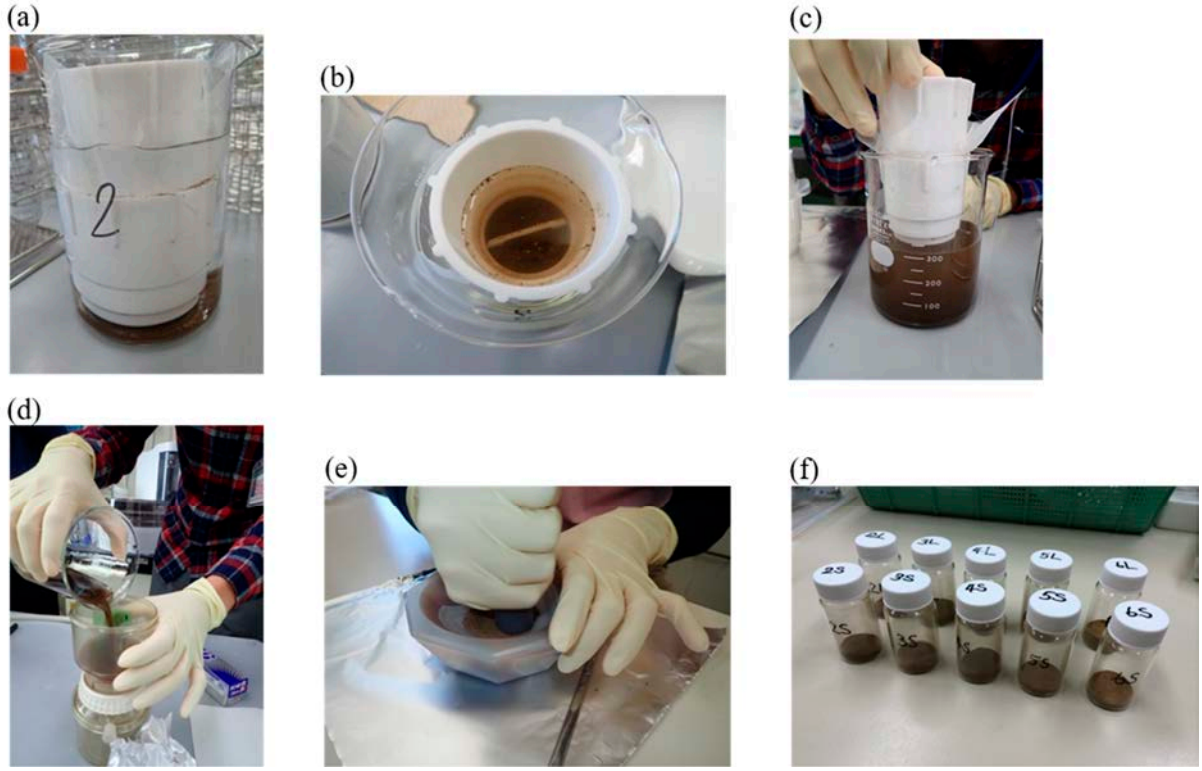

Fig. 4.4. Photos of the aggregate-size fractionation procedure: submersible sieving set with a cleaned sieve with mesh size of 250 μm (a); the top view of submersible sieving set (b); pulling up and down the sieving set 50 times for 2 min (c); filtration of microaggregate samples that were passed through the sieve and contained in the water (d); grinding both microaggregate and macroaggregate (collected on the sieve) samples (e); and the homogenized microaggregate and macroaggregate samples (f).

4.3. Chemical Fractionation

A chemical fractionation method is used to separate a soil sample into soil fractions according to different solubility and chemical reactivity of SOC. For example, acid hydrolysis is believed to remove compounds that are readily available to microorganisms, such as carbohydrates and proteins, while leaving more biologically recalcitrant materials[43,51]. Here, as an example, a simple method using acid and base solutions is described[4]. The flowchart of the chemical fractionation method is shown in **Fig. 4.5**.

Before starting fractionation, plant leaf fragments (PLF) are removed from soil samples by using tweezers, and are collected as a component of SOC for analysis. Approximately 2–7 g of the soil samples are hydrolyzed with 60 ml of 1.2M HCl at 80°C for 2 h. The suspension is centrifuged at 2000 rpm for 3 min and the supernatant is discarded. This treatment is repeated three times. The residue is then repeatedly washed with deionized water until the pH is > 4 to obtain acid-insoluble SOC fraction.

Subsample (~1–3 g) of the acid-insoluble fraction is further extracted with 60 ml of 1.2M NaOH at 80°C for 2 h, then the supernatant is decanted and replaced with fresh solution after centrifugation at 2000 rpm for 3 min. The extraction process is repeated until the supernatant become colorless. The residue is then washed with deionized water until the pH is < 10, treated three times with HCl to remove all carbonate contaminants, and repeatedly washed with deionized water as before to obtain insoluble SOC fraction[4].

Carbon content and ^{14}C isotope ratio are measured for the bulk (unfractionated) and two insoluble SOC fractions (**Fig. 4.5**). Using the measured values, C inventories and ^{14}C isotope ratios for the acid- and base-soluble SOC fractions can be quantified through mass balance calculations.

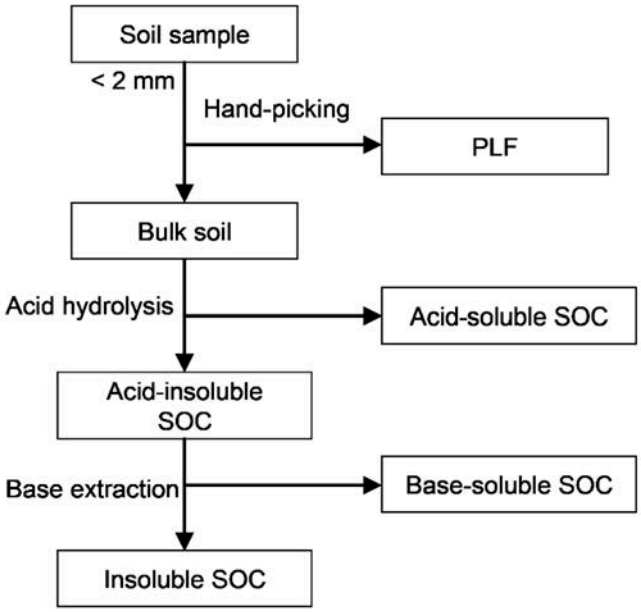

Fig. 4.5. Flowchart of the chemical fractionation method[4].

5. Analysis of Stable Isotopes

5.1. Stable Isotopes of Carbon and Nitrogen

Carbon and nitrogen have two stable isotopes each: ^{12}C and ^{13}C, and ^{14}N and ^{15}N. Their average natural abundances are 98.89% for ^{12}C and 1.11% for ^{13}C, respectively, for carbon isotopes, and 99.64% for ^{14}N and 0.36% for ^{15}N, respectively, for nitrogen isotopes. As the variation in the isotope composition in nature is exceedingly small for both carbon and nitrogen isotopes, the isotope composition is reported as a value relative to an internationally accepted standard and is generally expressed as the per mil (‰) deviation of the $^{13}C/^{12}C$ (or $^{15}N/^{14}N$) ratio of the sample from that of the standard, as follows:

$$\delta = [(R_{Sample}/R_{Std}) - 1] \times 1000 \quad \text{(Eq. 5.1)}$$

where R_{Sample} and R_{Std} are the ratios of the heavy to light stable isotopes ($^{13}C/^{12}C$ and $^{15}N/^{14}N$) in the sample and standard, respectively. The internationally accepted standards are Pee Dee Belemnite (PDB) for stable carbon isotopes and the atmosphere for stable nitrogen isotopes. Usually, working standards calibrated against the internationally accepted standards are used in routine measurements. Examples of the commercially available working standards are glycine (Lot No. AZ300M9R2283, Nacalai Tesque, Inc., $\delta^{15}N$ vs. air: 1.12 ± 0.2‰ and $\delta^{13}C$ vs. PDB: −32.3 ± 0.2‰) and L-alanine (Lot No. AZ100M6R397405, Nacalai Tesque, Inc., $\delta^{15}N$ vs. air: 5.0 ± 0.2‰ and $\delta^{13}C$ vs. PDB: −19.6 ± 0.2‰).

Here, an analytical method for the stable isotope ratios using isotope ratio mass spectrometry combined with elemental analysis is described; it has been used in the environmental science laboratory in the Japan Atomic Energy Agency (JAEA).

5.2. Configuration of the Measurement System

The carbon and nitrogen contents are measured using an elemental analyzer (EA, vario PYRO cube, Elementar, Germany), and the stable isotope ratios are measured using an isotope ratio mass spectrometer (IRMS, IsoPrime 100, IsoPrime, UK). The measurement system is shown in **Fig. 5.1**.

Soil samples are burned in a combustion furnace heated to 920°C in the vario PYRO cube, and the combustion products are passed through an oxidation catalyst by a constant flow of helium as a carrier gas (**Fig. 5.2**). The oxidation products are then passed through a reduction reactor. Copper granules within the reduction reactor reduce nitrogen oxides (NO, N_2O, and N_2O_2) to N_2. The CO_2 and N_2 are passed through a water trap and a CO_2 absorption column where CO_2 is separated from N_2 by controlling the temperature of the column. The N_2 and CO_2 are then passed through a thermal conductivity detector (TCD) sequentially and are sent to the IRMS. Generally, carbon content in soil

samples (soil organic matter) exceeds nitrogen content and therefore a diluter is used to reduce the amount of CO_2 to balance it with N_2. The CO_2 flow from the EA is injected into a helium flow in the diluter, and then a part of the CO_2 flow is introduced into the IsoPrime 100.

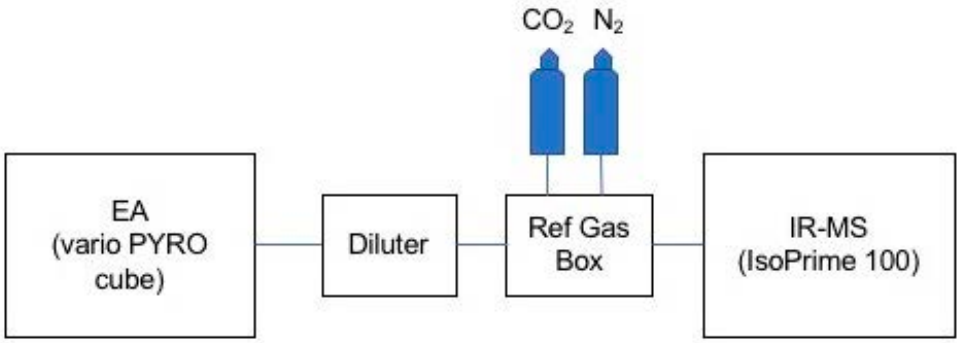

Fig. 5.1. The measurement system for stable carbon and nitrogen isotopes: IRMS connected to EA.

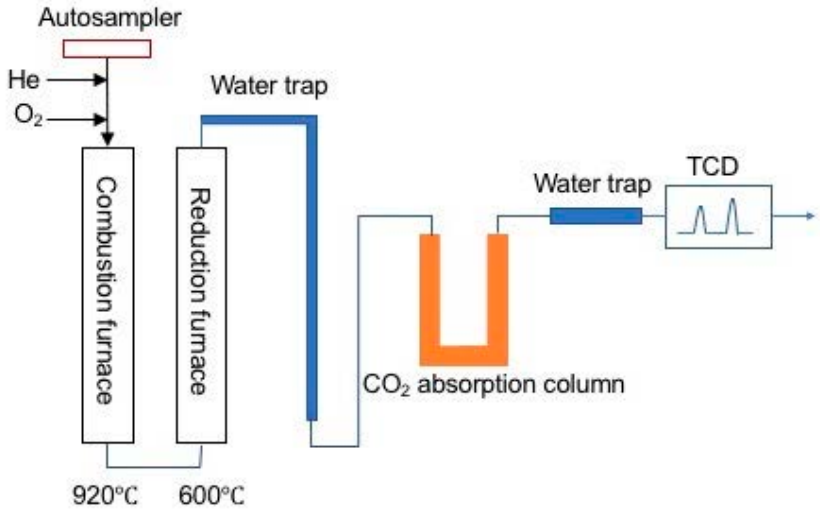

Fig. 5.2. The configuration of the vario PYRO cube.

The reference N_2, sample gas, and reference CO_2 can be introduced into the IsoPrime 100 in this order by switching the valve in the reference gas injector box ("Ref Gas Box" in **Fig. 5.1**). Then, stable isotope ratios of carbon and nitrogen are measured against a pulse of reference gas of known isotopic composition. The carbon and nitrogen isotopes in the sample gas are ionized at an electron impact source. The ions generated by the ion source are deflected by an electromagnet, separated by the mass, and finally detected simultaneously by a multi-collector.

5.3. Sample Preparation

Prepare what you need before work: aluminum foil on the work bench, several tweezers and micro-spatulas, tin boats of appropriate size, working standards, tungsten oxide powder, soil samples, and a 96-hole tray for wrapped samples. The samples must be dried and homogenized by grinding using a mortar and pestle. The powdered samples are stored in a closed container to prevent it from absorbing moisture. For the measurement, each of the samples is weighed and wrapped in a tin boat (**Fig. 5.3**). Several sizes of tin boat exist; the size of tin boat used here is 12 mm × 6 mm × 6 mm (height), and it can be changed depending on the carbon and nitrogen contents of the sample. To avoid contamination of the samples, the weighing area and all tools (tweezers, micro-spatulas, sample trays, and aluminum foil on the balance weighing pan) used for the weighing procedure must be kept clean. Wear gloves to avoid contamination from natural greases on the hands.

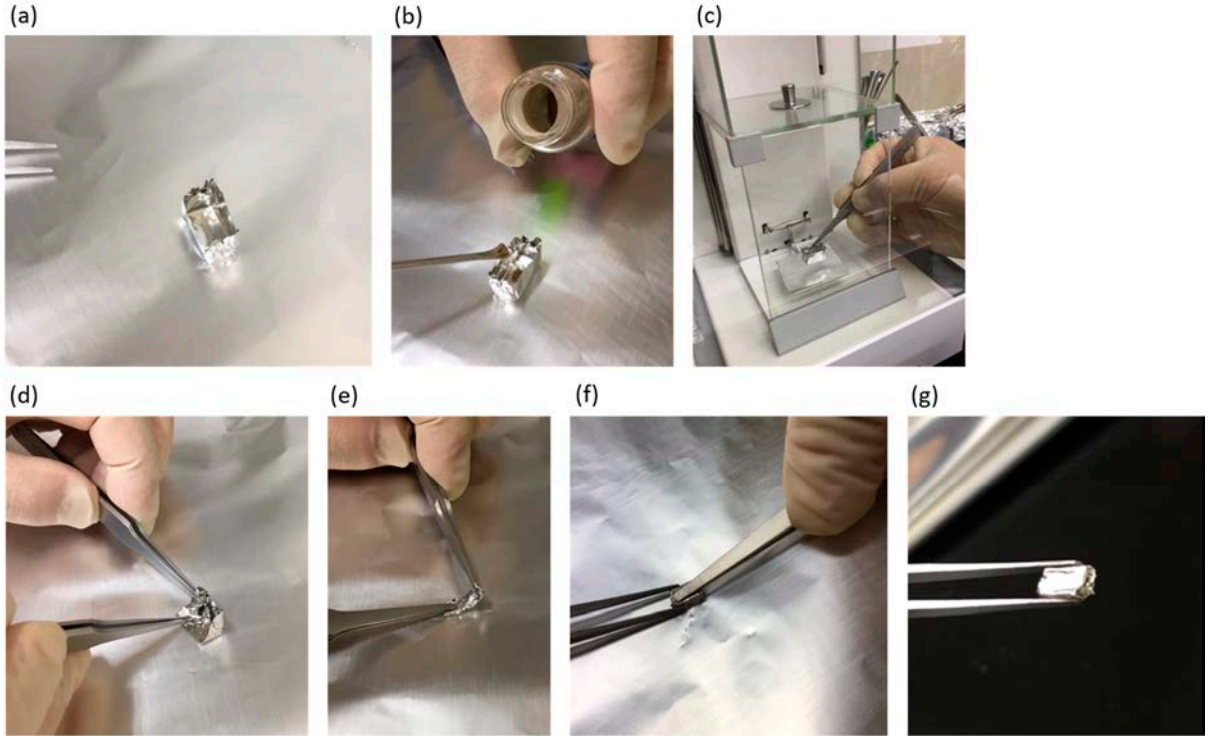

Fig. 5.3. Sample preparation procedure for stable isotope analysis: (a) a tin boat; (b) putting soil samples in the tin boat; (c) weighing; (d-f) enfolding the sample by the tin boat; and (g) a tin-wrapped sample for analysis.

First, as a blank sample, three new tin boats with no soil samples are crushed with tweezers to remove any air. Next, place a new tin boat on the pan of the microbalance and press the TARE button. Remove the tin boat from the balance pan and place a small amount of sample into the boat. Weigh the sample. If

necessary, adjust the sample weight by adding or removing some sample materials. Do not forget to record the weight. For soil samples, powdered tungsten oxide (equivalent to 1–3 times the sample weight) must be added as a combustion catalyst. Using the tweezers, close the top of the tin boat tightly and fold it over. Fold it several times in all directions and form it in a ball-like form. To avoid potential sample loss, take care not to damage the tin foil when folding. The resulting ball should be tightly packed to ensure that the sample is completely sealed inside the tin-foil ball to optimize the combustion process. The final geometry should be as spherical as possible to prevent any jamming inside the autosampler of the EA. A working standard is needed for every five or six unknown samples. Put the tin-wrapped ball-like sample in a tray and record the tray position number. Wrap the tray in Parafilm if it will take a long time from the sample preparation to measurement. Clean your tools and the work surface with Kimwipes and alcohol before moving to the next sample.

For the isotope ratio measurements, it is desirable to adjust the amounts of carbon and nitrogen in working standards and samples to be as equal as possible. It is, therefore, better to measure the amounts of carbon and nitrogen in samples before measuring the isotope ratios. If the IRMS is optimized and tuned well, the isotope ratios can be stably measured when the peak height is 2–10 nA. Since the relationship between the amounts of carbon and nitrogen and the peak height changes depending on the tuning, the condition of the device, and the setting of the diluter, it is better to determine the required sample weight after confirming the relationship by a preliminary measurement of the working standard.

5.4. Practical Procedure of the Measurement

[When returning from Sleep mode] Check the amount of helium remaining in the helium gas cylinder. Click the “Wake up now” button in the vario PYRO cube software (vario software) (Option > Settings > Sleep and Wake up) to make the EA standby and confirm that the furnace temperature and helium carrier flow rate have reached the specified values. Open the helium gas valve behind the diluter. After turning off the ion source in the Tune Page window of the IonVantage software (Option > Settings > Source On), open the Nupro valve. Wait until the vacuum gauge stabilizes at 2–6 × 10^{-6} mbar and the color of the bar in the display turns green. Then, turn on the ion source again. Confirm that the source status becomes “Operational” (green). To tune the acceleration voltage, click the “Run Peak Center” button in the Peak Center Results window for each reference gas and check the peak shape in the Peak Display window. Then, save the tuning file. Check the stability and linearity of the mass spectrometer.

Place the tin-wrapped sample in the sampler tray of the autosampler (**Fig. 5.4**). Open the document (or create a new one and name it) to be used for the measurement in the vario software. Open the sample list (or create a new one) in the IonVantage software. Enter the sample information in the sample list. Save the sample list. Select the line you want to run, and click the “Run” button. In the window that appears, confirm that the boxes before “Acquire Sample Data” and “Auto Process Samples” are checked,

and click the “OK” button. After the measurement, be sure to close the Nupro valve and then close the helium gas valve behind the diluter. Click the “Sleep now” button in the vario software.

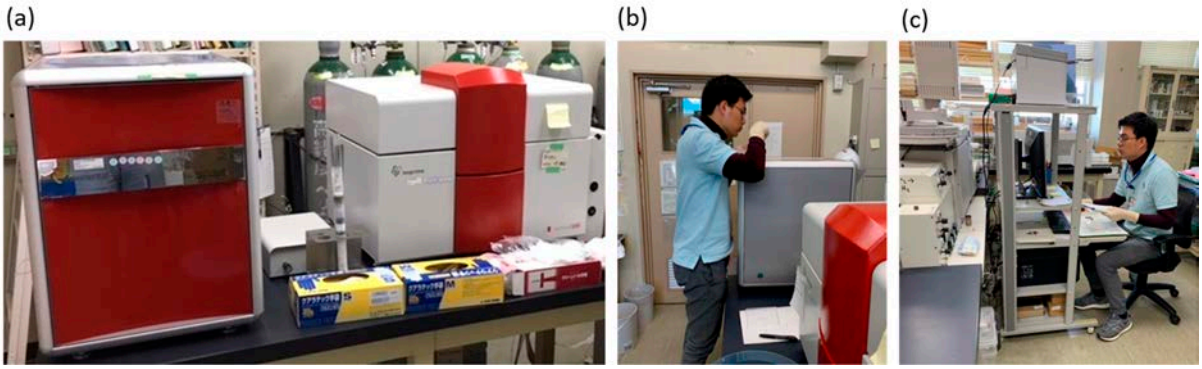

Fig. 5.4. Photos of the EA-IRMS system (a), putting the tin-wrapped sample in the autosampler of the EA (b), and operating softwares to measure stable isotope ratios of the samples (c).

5.5. Data Processing

Export the data of the TCD peak area in the EA measurement from the vario software. To calculate the amounts of nitrogen and carbon, calibration curves (to evaluate the amounts of nitrogen and carbon from the peak areas) are created based on the measurement results of a set of the working standard samples.

Data of the isotope measurements are collected from the data folder or batch file folder in the project file folder. The δ values in the data file need correction using the measurement results of the working standard samples. Confirm that the isotope ratio of the working standard does not vary largely before using these data.

6. Sample Preparation for Radiocarbon Analysis

Sample pretreatment is required for radiocarbon (^{14}C) measurement with the use of accelerator mass spectrometry (AMS). It includes: combustion of solid samples into gas samples; purification of CO_2 in the gas samples; conversion of CO_2 into graphite; and preparation of graphite targets for AMS. In this chapter, practical methods of sample preparation for AMS are briefly described.

6.1. Combustion of Soil Sample to Generate CO_2

Soil samples (equivalent to about 3–4 mg of carbon, but this depends on the AMS system to be used for ^{14}C measurement) are weighed into pre-combusted quartz tubes (6 mm in diameter, **Fig. 6.1**). Approximately 1 g of copper oxide (CuO) wire, 0.5 g of reduced copper wire, and Ag foil (approximately 5 cm × 4 mm) are also added into the tubes. The tubes are inserted into pre-combusted quarts tubes (9 mm in diameter), which are then attached to a multipurpose vacuum line. The vacuum line is equipped with pressure gauges and a vacuum gauge to continuously monitor the pressure in the line. The tubes are evacuated to a pressure of about 10^{-3} mbar and then flame-sealed. The samples in the sealed tubes are combusted at 500°C for 30 min and 850°C for 2 h[4].

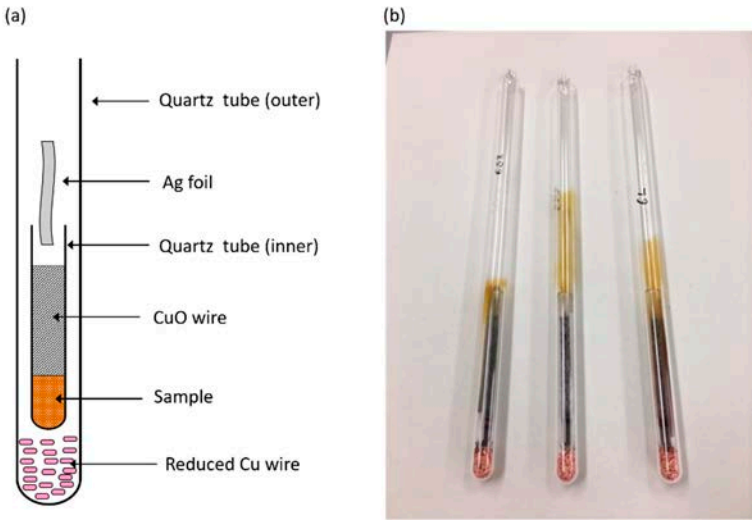

Fig. 6.1. Schematic diagram of the sample preparation for combustion (a) and photo of the combusted samples in the quartz tubes (b).

6.2. Purification of CO_2

The gas generated in the tubes by combustion is introduced into the vacuum line and CO_2 in the gas is cryogenically purified and then recovered (**Fig. 6.2**). The gas introduced into the line is passed through two multi-loop traps cooled with liquid nitrogen, in which CO_2 in the gas sample is completely trapped.

Molecular nitrogen (N_2), O_2 and other gaseous compounds in the gas sample are not trapped in these traps and pumped away. The CO_2 trapped in the first multi-loop trap is then liberated by changing the cooling agent from liquid nitrogen into liquid nitrogen-ethanol mixture (approximately −90°C) while water remains trapped in this trap. The CO_2 is then transferred to the second multi-loop trap that remains cooled with liquid nitrogen, and consequently, all CO_2 in the sample is trapped in the second trap. The CO_2 trapped in the second trap is liberated as before, and is transferred to a known-volume reservoir to quantify the amount of carbon by measuring the CO_2 pressure.

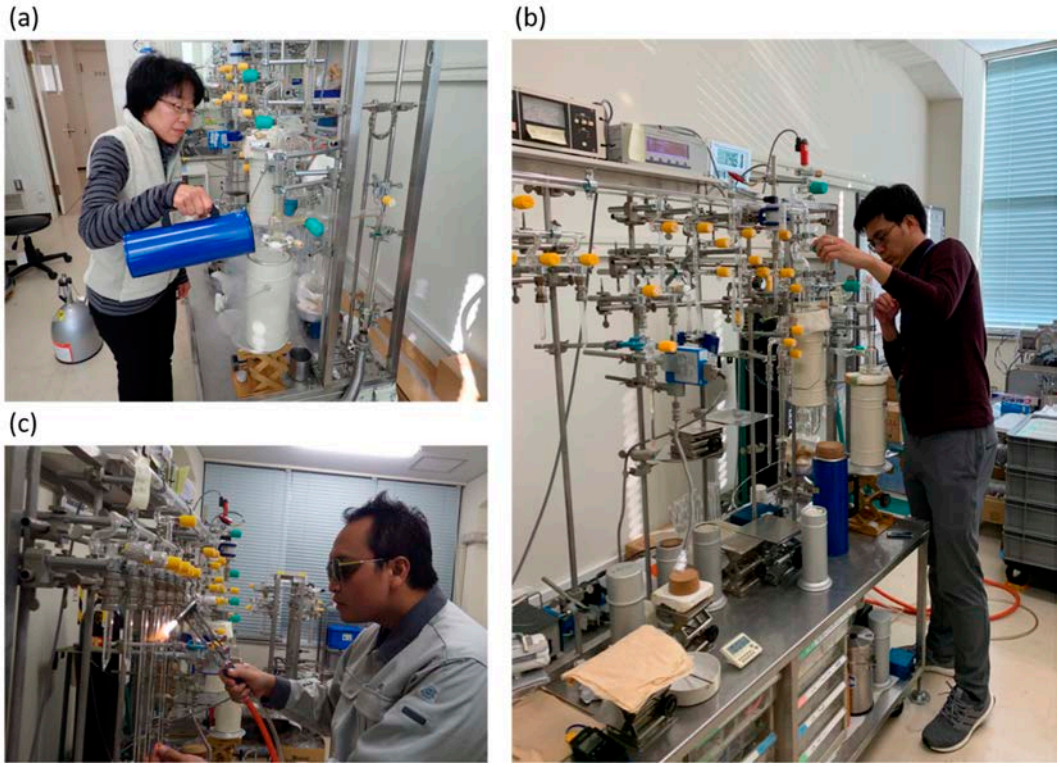

Fig. 6.2. Photos of the start-up of the vacuum line (a), the transfer of CO_2 to a trap cooled with liquid nitrogen (b), and flame-sealing of the purified CO_2 in the Pyrex glass tube (c).

Finally, the purified CO_2 is separated into two fractions: one is for ^{13}C analysis with the IRMS (approximately 1 mg of carbon as CO_2) and the other is for ^{14}C measurement with the use of AMS. This is conducted by expanding the CO_2 in two known-volume areas in the line for 5 min. Each of the fractions (CO_2 in the two known-volume areas) is transferred to a pre-combusted Pyrex glass tube cooled with liquid nitrogen and flame-sealed. Note that each of the gas transfer processes requires approximately 3 minutes to allow the CO_2 transfer to complete.

6.3. Conversion of CO_2 into Graphite

For ^{14}C measurement with the use of AMS, it is necessary to prepare a graphite target. A number of graphitization methods have been developed and they rely on reduction of CO_2 in the presence of a catalyst. The hydrogen reduction method is the most widely used method for graphite production from CO_2[60–62]. The net reaction is:

$$CO_2 + H_2 \rightarrow H_2O + C \text{ (graphite)} \qquad \text{(Eq. 6.1)}$$

The CO_2 reduction is achieved in a reaction tube made by Pyrex glass (**Fig. 6.3**). A small cup (made by Vycor glass with high-temperature resistance) is placed inside the reaction tube; the small cup contains iron powder which works as a catalyst (**Fig. 6.3**). The iron powder in the cup is pre-cleaned and reduced with H_2 gas at 450°C. Part of the purified CO_2 and H_2 gases (CO_2 : H_2 = 1 : 2.5) are transferred into the reaction tube using a vacuum system (**Fig. 6.4**). After that, the reaction tube (and a water trap tube directly connected to the reaction tube) is sealed and separated from the vacuum system, and is set to an electric heating furnace for CO_2 reduction (**Fig. 6.5**). The electric heating furnace is run at 650°C within 10–12 h including a cooling time. Water generated during the reaction in the tube is removed by the water trap tube which is cooled at the upper part of the electric heating furnace.

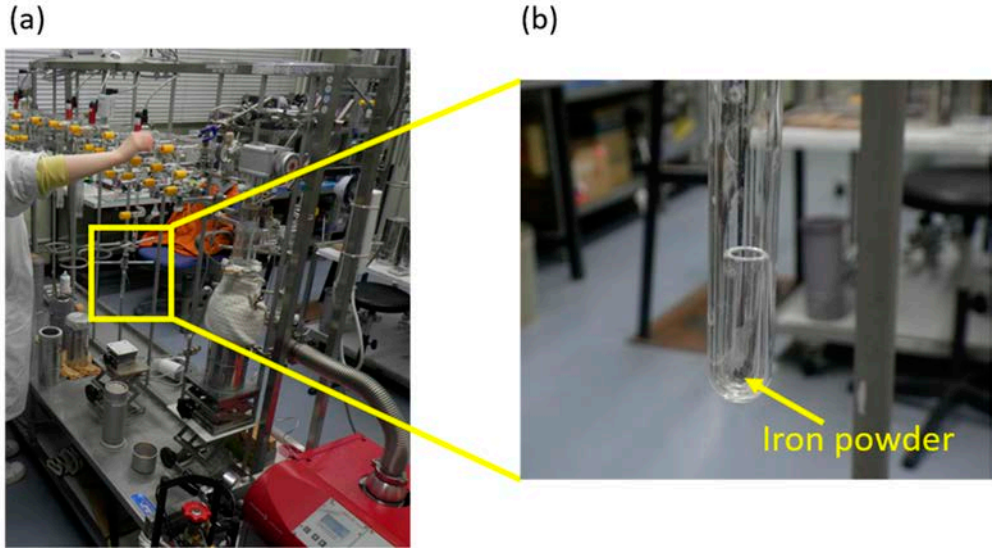

Fig. 6.3. Photos of the vacuum system (a) and a small cup with iron powder placed inside the reaction tube (b).

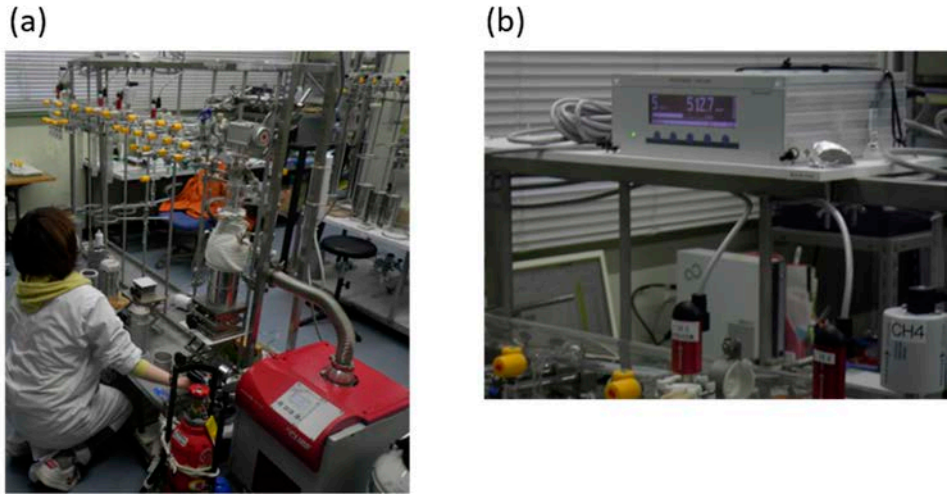

Fig. 6.4. Photos of the procedure of filling H_2 gas in a reaction tube containing CO_2 sample and iron powder (a) and a vacuum gauge to quantify the amount of H_2 gas transferred to the reaction tube (b).

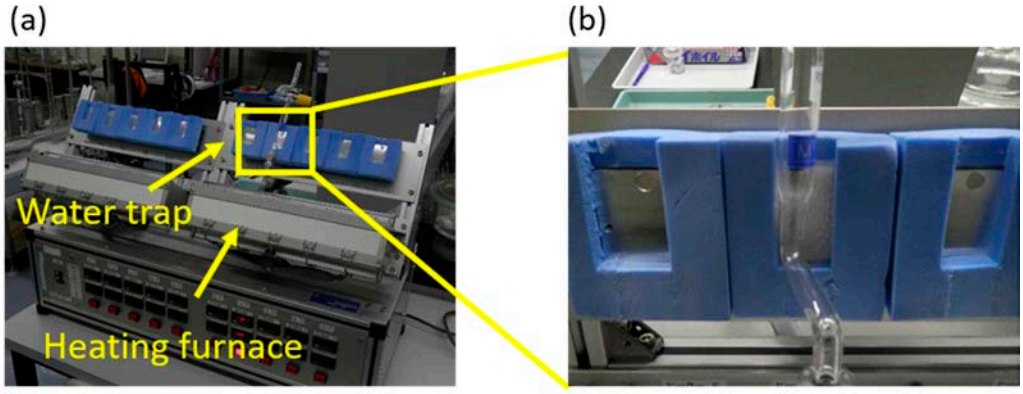

Fig. 6.5. Photos of the reduction of CO_2 to graphite in a reaction tube using an electric heating furnace (a) and a water trap to remove water generated during the reduction (b).

6.4. Preparation of Graphite Target

At the AMS facility of the Aomori Research and Development Center of JAEA, for example, the target piece is set in a target press tool and then the graphite sample goes through the funnel to the top of the target piece (**Fig. 6.6**). A back pin is inserted into the target piece from the back side and then the back pin is pressed by a press machine. As a result, the graphite sample is set to the surface of the target piece. After confirming that the surface of the target piece is clean, target pieces are arranged in the order of measurement. These processes are carried out under a clean bench to avoid any contamination.

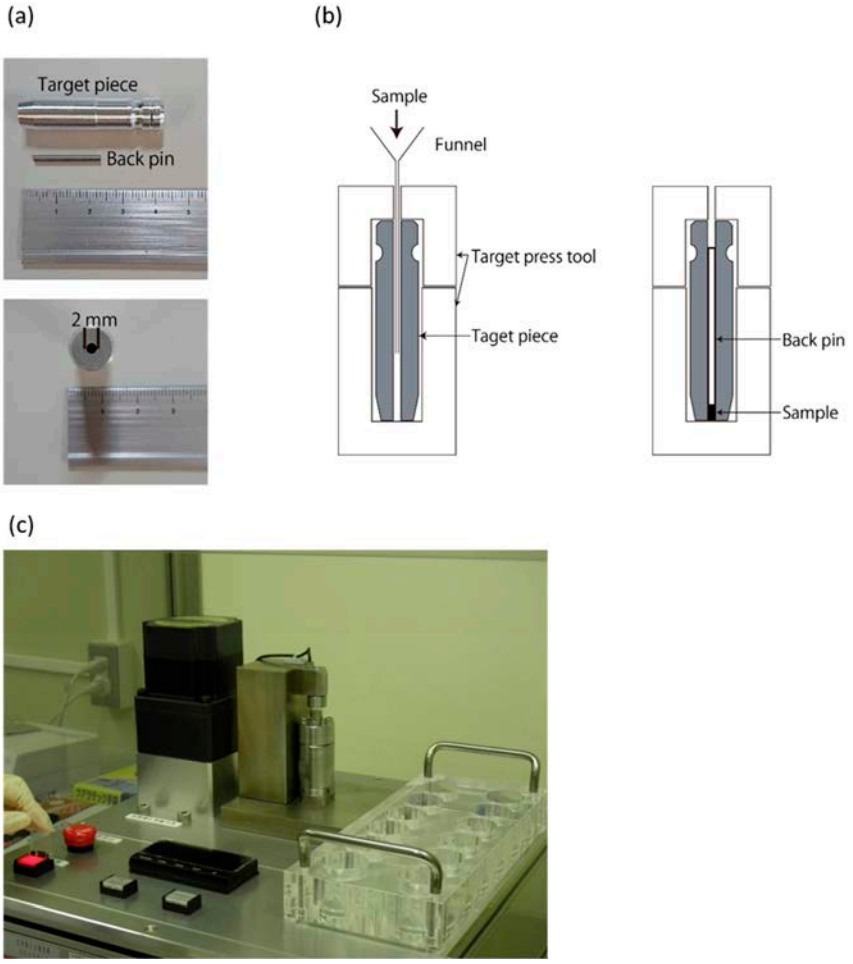

Fig. 6.6. Photos of a target piece (a), schematic diagram of setting graphite sample in the target piece (b), and photo of the loading of graphite into a target piece by using a press machine (c).
This target piece is one used at the JAEA-AMS-MUTSU.

6.5. A Recent Advance in the Sample Preparation Method

A new graphitization system has recently been developed and employed to rapidly and efficiently prepare samples for AMS-^{14}C measurement. The graphitization system relies on an Automated Graphitization Equipment (AGE3, Ionplus AG, Switzerland) directly coupled to an elemental analyzer (EA). AGE3 uses a molecular sieve trap, instead of a cryogenic trap, to isolate CO_2 from the combustion gas[63]. The samples (wrapped in a tin boat as in the stable isotope analysis, see Section 5.3) are combusted in the EA, and the resulting CO_2 in the combustion gas is adsorbed in a column filled with zeolite material. Afterwards, the CO_2 is thermally released from the column and transferred to a graphitization reactor in the AGE3. This system has now started operation at the AMS facility of the Tono Geoscience Center of JAEA[64].

7. Radiocarbon Analysis by Accelerator Mass Spectrometry

7.1. Radiocarbon

Radiocarbon (^{14}C), the radioactive isotope of carbon, is a cosmogenic radionuclide and is therefore constantly being generated by the interaction of cosmic rays with nitrogen isotope (^{14}N) in the atmosphere. The ^{14}C nuclei is unstable and decays back to ^{14}N by emitting a β particle, with the physical half-life of 5730 years. The ^{14}C nuclei generated in the atmosphere is oxidized to $^{14}CO_2$ (the form of carbon dioxide) in a matter of a few months. The $^{14}CO_2$ mixes into the troposphere and enters the global carbon cycle that continuously exchanges carbon between atmosphere, terrestrial, and ocean carbon reservoirs. The natural abundance of ^{14}C is roughly one in every trillion (10^{12}) carbon atoms (an abundance of ~10^{-10}%) in the environment[65].

7.2. Accelerator Mass Spectrometry

Accelerator mass spectrometry (AMS) is an excellent technique to measure ^{14}C in environmental samples (including soil samples and soil organic carbon fractions), because of the low detection limit, good precision, small sample volume required, and short measurement time. Here, we introduce three of the AMS systems operating in Japan: JAEA-AMS-MUTSU, JAEA-AMS-TONO-5MV, and MALT-AMS.

7.2.1. JAEA-AMS-MUTSU

The accelerator mass spectrometer (AMS) at the Aomori Research and Development Center of JAEA (JAEA-AMS-MUTSU) is based on a 3 MV Tandetron system (Model 4130, High Voltage Engineering Europe). JAEA-AMS-MUTSU has two beamlines: one is optimized for ^{14}C measurement and the other is for ^{129}I measurement. The AMS is equipped with a simultaneous injection system for high-precision ^{14}C measurement[60]. Photo and schematic layout of JAEA-AMS-MUTSU are shown in **Fig. 7.1**. At the negative ion source for the ^{14}C measurement, negative carbon ions (C^-) are produced by the cesium (Cs) sputtering. Molecular ions ($^{12}CH^{2-}$, $^{13}CH^-$) which are isobar of ^{14}C are also produced. Accelerated negative carbon ions and molecular ions collide with Ar gas which is installed at the center of the accelerator. Outermost electrons of negative carbon ions are stripped by this collision and molecular ions are broken and also stripped by this collision. Therefore, negative carbon ions and molecular ions become positive ion ($^{12}C^{n+}$, $^{13}C^{n+}$, $^{14}C^{n+}$). After passing through the accelerator, positive carbon ions can be separated by the analyzing magnet. Finally, only the target ion (^{14}C) can be introduced into the ionization detector and then counted, whereas ^{12}C and ^{13}C ions can separately be detected by Faraday cup detectors.

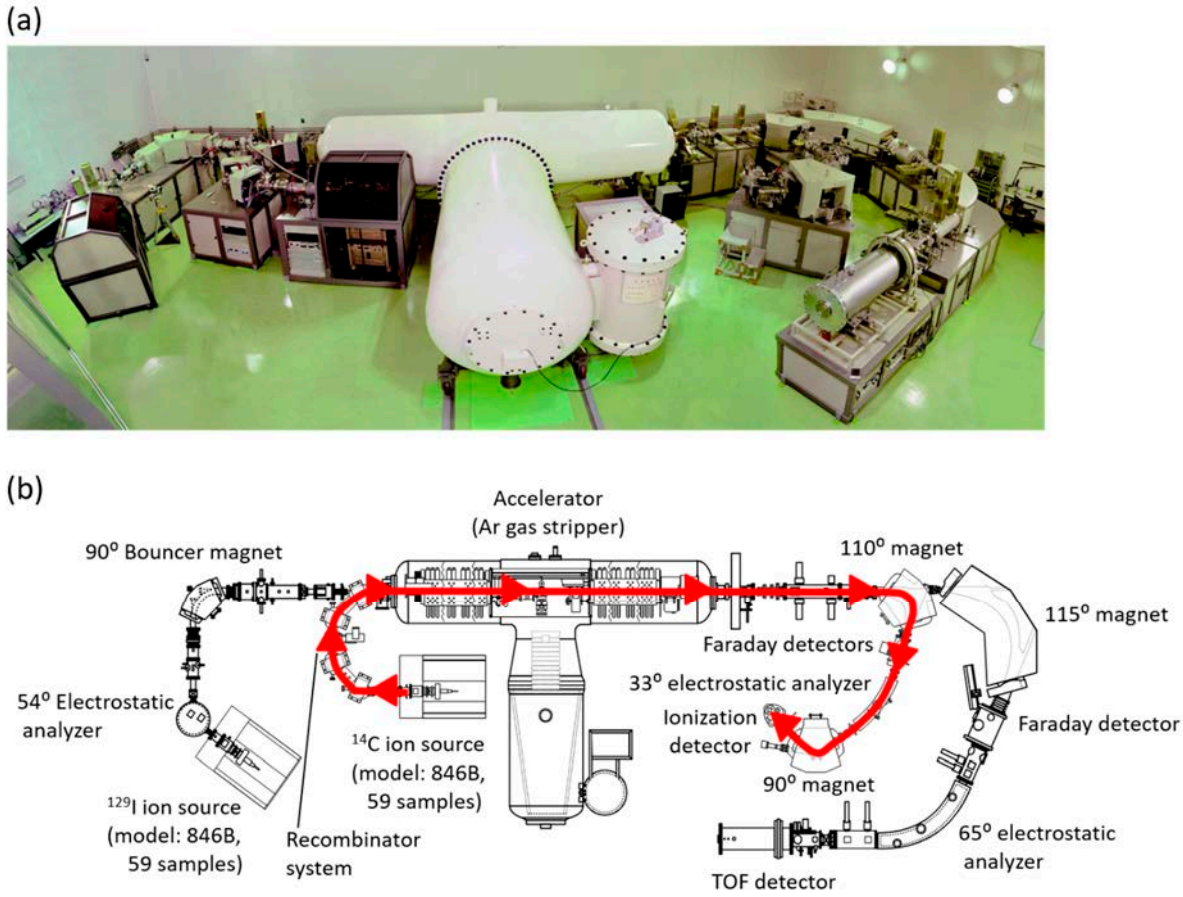

Fig. 7.1. Photo (a) and schematic layout (b) of the JAEA-AMS-MUTSU system.
A beamline on red is optimized for ^{14}C measurement.

7.2.2. JAEA-AMS-TONO-5MV

The AMS at the Tono Geoscience Center of JAEA (JAEA-AMS-TONO-5MV) is a multi-nuclide system based on a 5 MV tandem Pelletron type accelerator (Model: 15SDH-2) by National Electrostatics Corporation, USA[64,66]. One beamline of the AMS enables us to measure not only ^{14}C but also other nuclides such as ^{10}Be, ^{26}Al, and ^{129}I. Schematic layout of the JAEA-AMS-TONO-5MV is shown in **Fig. 7.2**. The AMS has two ion sources: a 40-target MC-SNICS ion source and a 12-target MGF-SNICS. Currently, only the MC-SNICS is used, and the MGF-SNICS is not used. Low energy side of the AMS beamline is equipped with a 90° double focusing injection magnet producing fast sequential isotope injection for multi-nuclide measurement. High energy side of the AMS beamline is equipped with a 90° double focusing analyzing magnet, multi-Faraday cup detector system, a 20° electrostatic cylindrical analyzer, and an ionization detector. The two Faraday cup detectors and the ionization detector are used for measurements of ^{12}C,^{13}C, and ^{14}C, respectively. The ionization detector consists of a cathode

electrode, grid and anodes of five ΔE electrodes[67]. This has a beneficial effect on discrimination between isobars and enables us to detect multi nuclides by using the single beamline.

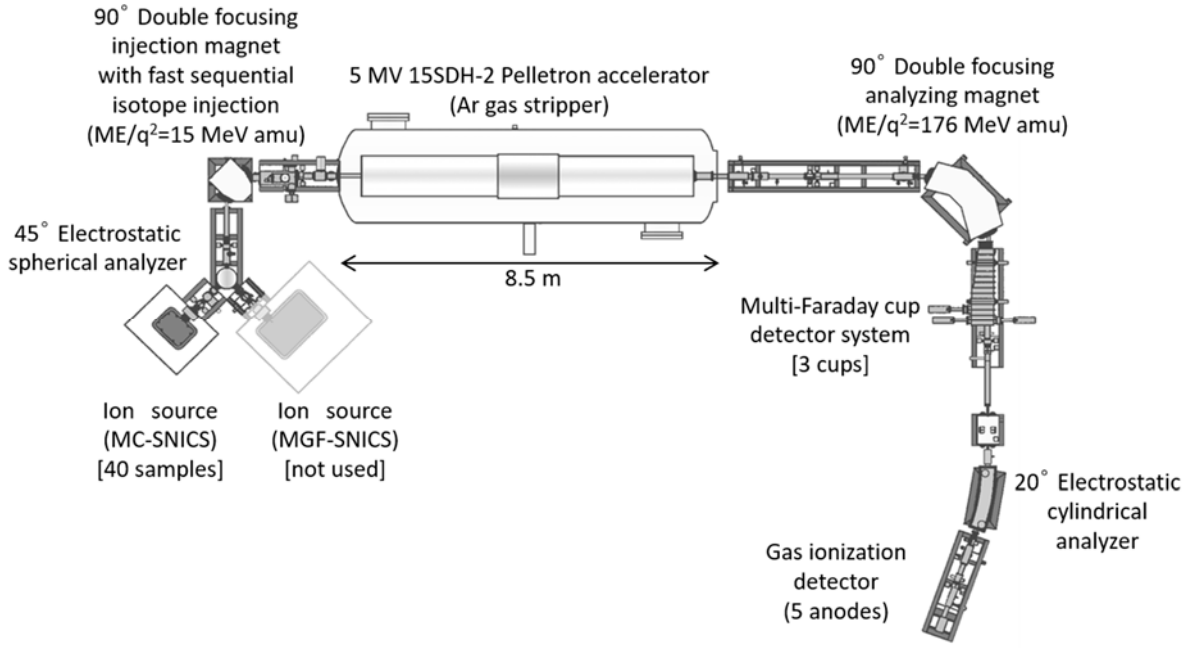

Fig. 7.2. Schematic layout of the JAEA-AMS-TONO-5MV system.

7.2.3. MALT-AMS

The AMS at the Micro Analysis Laboratory, Tandem accelerator, the University of Tokyo (MALT-AMS) is based on a Pelletron 5UD tandem accelerator by National Electrostatics Corporation, charged by a pellet chain up to 5 MV[68]. MALT-AMS comprises a Cs-sputter ion source, a sequential injection system, and multi-Faraday cup system for high precision AMS measurements. There are several beam courses such as NRA (nuclear reaction analysis) and PIXE (particle induced X-ray emission), in addition to AMS course, at MALT-AMS (**Fig. 7.3**).

A new method for ^{14}C-AMS has been used at MALT-AMS in which only beams with mass 13 and 14 are injected into the accelerator. In this method, $^{14}C/^{13}C$ is measured by ^{14}C counts at the final detector and $^{13}C^{4+}$ current by MFC 04-2 (one of multi Faraday cups). $^{13}C/^{12}C$ is evaluated from the current ratio of $^{13}C^{4+}$ generated at the terminal from $^{13}CH^-$ (mass 14) and $^{12}C^{4+}$ generated from $^{12}CH^-$ (mass 13) measured by MFC 04-1 and MFC 04-4, respectively. All three stable isotope beams, $^{13}C^{4+}$ from $^{13}C^-$, $^{13}C^{4+}$ from $^{13}CH^-$ and $^{12}C^{4+}$ from $^{12}CH^-$, come to different positions after the analyzing magnet so that three offset Faraday cups are needed for the simultaneous measurements with sequential injection of

mass 13 and 14. Using this method, $^{13}C/^{12}C$ can be measured reasonably[69].

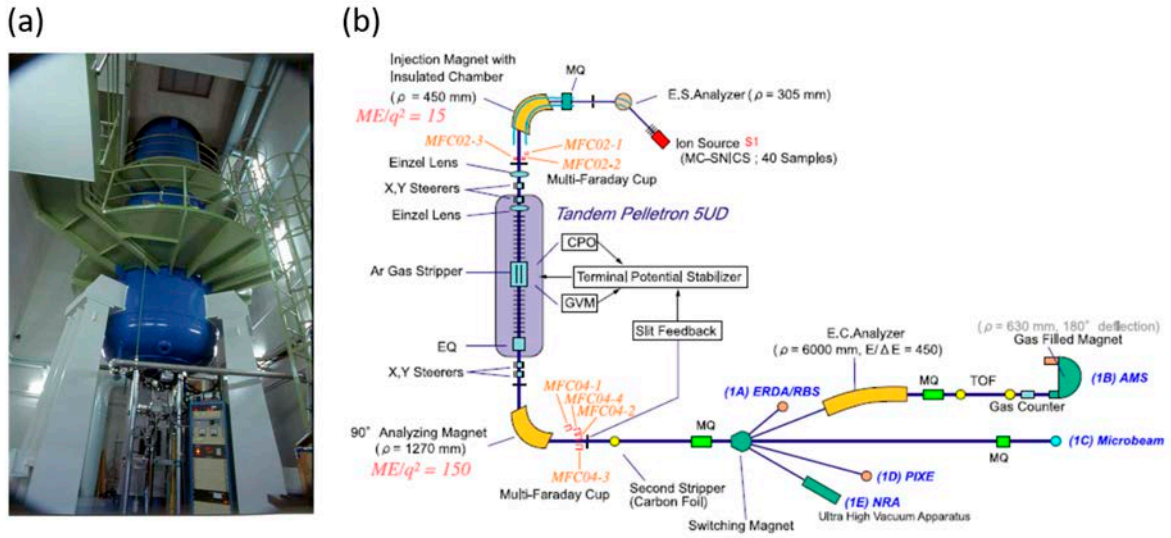

Fig. 7.3. Photo of the accelerator (a) and schematic layout (b) of the MALT-AMS system.

7.3. Reporting Radiocarbon Data

There are several ways to report radiocarbon (^{14}C) data depending on the application[65,70]. As with stable isotopes, ^{14}C data are reported based on comparing the $^{14}C/^{12}C$ of the sample to that of a universal standard. Two factors are to be considered, however, to report ^{14}C data: corrections of mass-dependent isotope fractionation and radioactive decay. Regarding the mass-dependent isotope fractionation, the $^{14}C/^{12}C$ ratios are corrected for mass-dependent isotope fractionation based on stable carbon isotope ratios ($^{13}C/^{12}C$), assuming that the mass-dependent fractionation of ^{14}C in relation to ^{12}C is twice as large as that of ^{13}C during carbon cycling (biochemical and physical) processes. Regarding the radioactive decay, the $^{14}C/^{12}C$ ratios in the standard used for the AMS measurement decrease over time as the ^{14}C in the standard is subjected to radioactive decay. This is corrected by selecting a specific time (1950 in the case of ^{14}C) and decay to take into account the ^{14}C lost between 1950 and the year the standard was measured[65].

Two ways to report ^{14}C data are briefly described below, which are frequently used for carbon cycle studies.

7.3.1. Radiocarbon age

Like stable carbon isotopes (^{12}C and ^{13}C), ^{14}C enters the terrestrial ecosystems by uptake of atmospheric CO_2 through photosynthesis. During its lifetime, organisms remain in isotopic equilibrium with the

atmosphere due to the quick exchange of C between them. Immediately after the organisms die, however, the ^{14}C isotope ratio ($^{14}C/^{12}C$) in the organisms (organic matter such as plant tissues in this case) starts to decrease as a result of the radioactive decay of ^{14}C with a physical half-life of 5730 years. Therefore, measuring the ^{14}C isotope ratio of a sample enables us to estimate the age of the organic matter in the sample by comparing it with the ^{14}C isotope ratio of a standard with known age. This is well known as ^{14}C dating. The ^{14}C isotope ratio of the atmospheric CO_2 in 1950 is generally used as a standard for this purpose.

Conventional ^{14}C age (in years BP; BP means before present with present defined as 1950) is reported as:

$$^{14}C \text{ age} = -8033 \cdot \ln(A_0/A) \qquad \text{(Eq. 7.1)}$$

where 8033 is the mean life of ^{14}C (= 5568/ln2 in years) based on the Libby half-life (5568 years, this value is still used by convention for reporting the ^{14}C age, although the half-life value has been updated as before), A_0 is the initial $^{14}C/^{12}C$ ratio of the sample which is defined by reference to the 1950 standard, and A is the $^{14}C/^{12}C$ ratio of the sample. If A is smaller than A_0, then A can give an estimate of the time elapsed since the sample was isolated from exchange of ^{14}C (and ^{12}C) with the atmosphere. Note that the ^{14}C dating assumes that there has been no loss (other than radioactive decay) or addition of ^{14}C to the sample since it ceased exchanging with the atmosphere (i.e., since death of the organism).

7.3.2. $\Delta^{14}C$

The absolute amount of ^{14}C in a sample in the year it was measured can be more informative particularly for geochemical applications. In this case, a correction for radioactive decay undergone by the standard between 1950 and the year the sample was measured must be done, and ^{14}C value for the sample is reported as:

$$\Delta^{14}C = [R_{sample,-25}/\{0.95 \times R_{OXI,-19} \times \exp((y-1950)/8267)\} - 1] \times 1000 \qquad \text{(Eq. 7.2)}$$

where $R_{sample,-25}$ is the $^{14}C/^{12}C$ ratio of the sample normalized to the common $\delta^{13}C$ value of −25‰ to account for the mass-dependent isotopic fractionation, $R_{OXI,-19}$ is the $^{14}C/^{12}C$ ratio of the OX-I standard normalized to $\delta^{13}C$ value of −19‰, and y is the year the sample was measured. The term $0.95 \times R_{OXI,-19}$ represents the internationally accepted ^{14}C reference value in 1950, and the following exponential term is for decay correction for change in the OX-I standard since 1950. Note that in this case of decay correction, the half-life of 5730 years, not the Libby half-life, is used, so that 8267 is the mean life of ^{14}C (= 5730/ln2 in years).

The notation $\Delta^{14}C$ is per mil (‰, or parts per thousand) deviation of the sample from the standard. Positive $\Delta^{14}C$ value indicate that the sample has more ^{14}C than the atmospheric CO_2 in 1950, indicating the presence of bomb-^{14}C[4,20,65]. A $\Delta^{14}C$ value of +1000‰ would be equivalent to a doubling of the $^{14}C/^{12}C$ ratio in the atmosphere, which is roughly the value reached in 1964 for atmospheric CO_2 owing to the atmospheric weapons testing[22].

8. Practical Application

This chapter demonstrates an application using ^{14}C and stable carbon and nitrogen isotopes to studying soil carbon dynamics, which was conducted in a Japanese temperate forest. The chapter includes: soil sampling and treatment; soil organic carbon fractionation by two methods (density and aggregate-size); stable isotope and ^{14}C analysis; and results obtained and their interpretations.

8.1. Soil Sampling and Treatment

Soil sampling was conducted at a 30-year-old evergreen broadleaved forest site in Tsukuba (in the premise of the National Institute for Environmental Studies, NIES) in November 2018 (**Fig. 8.1**). The method used for soil sampling was the soil-digging method (see Chapter 2). This is because the soil at this forest site has been classified as Andosol and is assumed to accumulate a significant amount of SOC even in deeper soil layers; therefore, we want to evaluate it throughout the soil profile. Litter samples was collected from O horizon (forest-floor litter layer) in the area of 30 cm × 30 cm, and thereafter, soil samples of five soil layers (0–10, 10–20, 20–30, 30–40, and 40–50 cm) were collected from a face of the pit. To determine the bulk density of the soil, we also collected soil samples from each of the soil layers, by using a known-volume (100 cm^3) soil sampler.

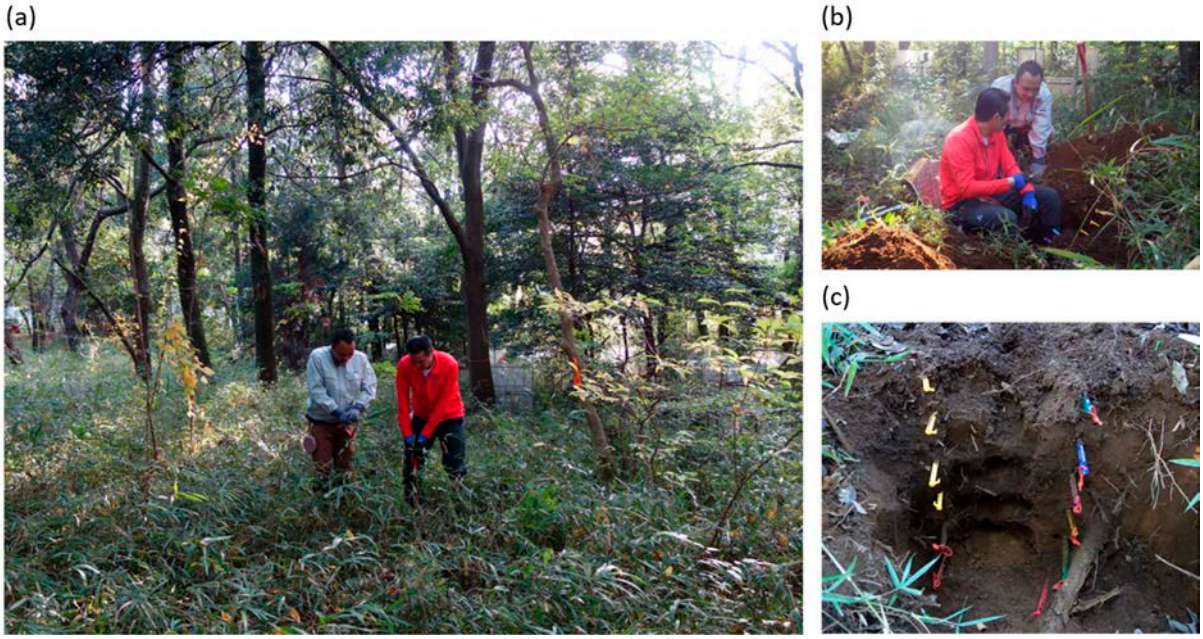

Fig. 8.1. Photos of the forest site in Tsukuba (a), soil sampling (b), and the face of the soil pit after sampling (c).

The litter and soil samples were immediately transported to the laboratory and then dried to a constant weight at room temperature. The litter samples were finely chopped using a mixer to obtain homogenized samples after removing coarse woody debris (fallen branches and twigs). The soil samples were sieved through a 2-mm mesh, and for analysis, the < 2 mm fractions were ground into powder in a mortar after carefully removing fine roots in the samples.

The soil samples of the 100-cm^3 volume were also dried, weighed, and sieved through a 2-mm mesh. Both fractions obtained by sieving (i.e., > 2 mm and < 2 mm fractions) were weighted to evaluate the bulk density and the gravel (> 2 mm) content of the soil.

8.2. Soil Organic Carbon Fractionation

To investigate the physical status of SOC and its relation to the SOC dynamics in the soil profile, we applied two fractionation methods. The density and aggregate-size fractionation methods, described in Sections 4.1 and 4.2, were applied to the soil samples. Through the density fractionation method, we separated the soil samples into two SOC fractions: a low-density fraction (LF: < 1.6 g cm^{-3} in density) and a high-density fraction (HF: > 1.6 g cm^{-3}) (**Fig. 8.2**). Through the aggregate-size fractionation, we separated the soil samples into two SOC fractions: macroaggregate fraction (MAA: > 250 μm in size) and microaggregate fraction (MIA: < 250 μm) (**Fig. 8.3**).

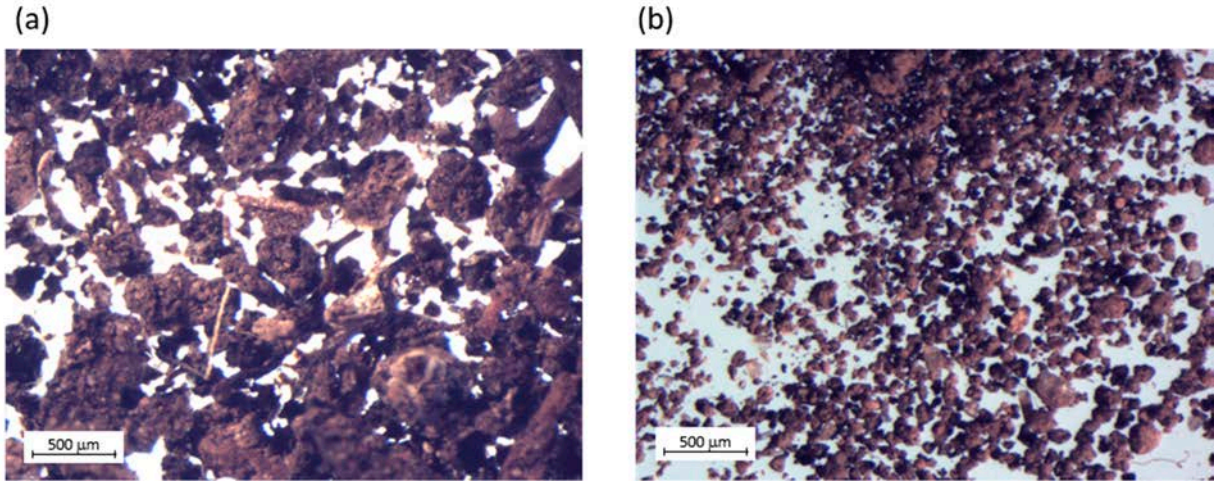

Fig. 8.2. Examples of LF (a) and HF (b) fraction samples isolated from the topmost (0–10 cm) soil layer observed using a stereomicroscope (SZX7, OLYMPUS, Japan). The LF fraction was dominated by plant detritus or particulate organic matter (POM), whereas the HF fraction was dominated by soil mineral particles.

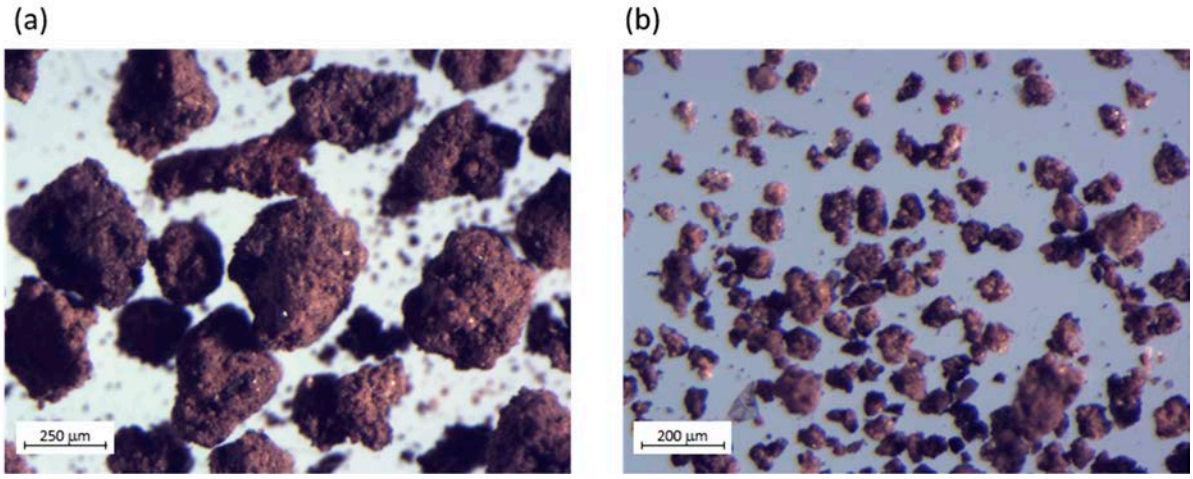

Fig. 8.3. Examples of MAA (a) and MIA (b) fraction samples isolated from the topmost (0–10 cm) soil layer observed using a stereomicroscope (SZX7, OLYMPUS, Japan). The MAA fraction was dominated by macroaggregates (> 250 μm in size), whereas the MIA fraction was dominated by microaggregates (< 250 μm).

8.3. Stable Isotope Analysis

A portion of each of the samples (litter, bulk soil, and SOC fractions) was analyzed for their total C and N contents using an elemental analyzer (vario PYRO cube, Elementar, Germany). Stable carbon and nitrogen isotope ratios ($\delta^{13}C$ and $\delta^{15}N$, respectively) were analyzed using an isotope ratio mass spectrometer (IsoPrime100, Isoprime Ltd., UK) connected with an elemental analyzer (vario PYRO cube), with an analytical uncertainty of < 0.1‰ (1SD). See Chapter 5 for detailed procedures of the stable isotope analysis.

8.4. Radiocarbon Analysis

Radiocarbon analyses were made with the JAEA-AMS-MUTSU for the bulk soil samples and the JAEA-AMS-TONO-5MV for the SOC fraction samples, respectively. The bulk soil samples were prepared for AMS-^{14}C measurements in the manner described in Sections 6.1–6.4. Briefly, the samples were combusted to generate CO_2 in evacuated quartz tubes with CuO, and the resulting CO_2 was cryogenically purified. Graphite targets for AMS were formed on fine iron power by reducing the purified CO_2 with hydrogen gas. To prepare the SOC fraction samples for AMS-^{14}C measurements, we used the automated graphitization system at the Tono Geoscience Center of JAEA (see Section 6.5).

8.5. Results and Interpretations

8.5.1. Carbon content and SOC stock

Results of the soil sampling and treatment and the measurement of C content in the soil samples are shown in **Table 8.1**. The SOC stock in the O horizon (litter layer) was evaluated using the equation (Eq. 3.2), based on the measured data of the litter inventory and C content of the litter sample. The SOC stock in each of the soil layers was evaluated using the equation (Eq. 3.1), based on the measured data of the bulk density, gravel content, and C content of the soil sample.

Table 8.1. Properties and SOC stocks in the O horizon and soil layers.

Layer	Litter inventory[a] (kg m^{-2})	Bulk density[b] (g cm^{-3})	Gravel content[c] (%)	C content (gC g^{-1} soil)	SOC stock (kgC m^{-2})
O (litter)	2.93	NA	NA	224	0.65
0–10 cm	NA[d]	0.52	2.5	86	4.30
10–20 cm	NA	0.53	0.7	52	2.74
20–30 cm	NA	0.48	0	42	2.04
30–40 cm	NA	0.47	0	31	1.45
40–50 cm	NA	0.52	0	22	1.13

[a]Litter inventory was evaluated from the dry weight of the litter sample in the collection area of 30 cm × 30 cm.
[b]Bulk density was evaluated from the dry weight of soil sample collected by the 100-cm^3 volume sampler.
[c]Gravel content was determined as a percentage by mass of the > 2 mm fraction of the 100-cm^3 volume sample.
[d]NA: Not available.

The bulk density of the soil was very low and fairly uniform throughout the soil profile. There was virtually no coarse particles (> 2 mm in diameter) in all soil layers. The litter sample showed a high content of C (224 gC g^{-1}), indicating a relatively small contribution of soil mineral particles in the O layer. The C content of the soil decreased with depth, and as a result, the SOC stock decreased with depth. The total stock of SOC in the first 20 cm of soil was determined to be 7.0 kgC m^{-2} for this forest site, which was approximately 1.4 times greater than the global average of SOC stock (5.1 kgC m^{-2})[71]. These properties are attributable to the unique physical and chemical properties of Andosol, which develops from parent materials of volcanic origin (volcanic ash). The large accumulation of SOC in this soil is probably due to the formation of organometallic complexes (Al-humus complexes) that resist microbial decomposition[72].

Carbon contents of the density and aggregate-size fractions are given in **Table 8.2**, together with that of the bulk soil. Regarding the desntity fractionation, the C content of the LF fraction was higher compared with that of the bulk soil, whereas the C content of the HF fraction is lower. The results indicate that the density fractionation is useful to separate the soil into two different SOC pools with different properties: the LF fraction is a particulate organic matter (POM)-dominant fraction with relatively free of mineral materials (soil particles), and the HF fraction is a mineral-dominant fraction. It is interesting to see that the C content of the LF fraction does not change so much with soil depth, even though the C contents of the bulk soil and HF fraction decrease with soil depth.

Table 8.2. Carbon content (in gC g^{-1} soil) of the bulk soil, density fractions, and aggregate-size fractions.

Layer	Bulk	Density fractions[a]		Aggregate-size fractions[b]	
		LF	HF	MAA	MIA
O (litter)	224	NA[c]	NA	NA	NA
0–10 cm	86	150	67	84	76
10–20 cm	52	140	45	45	50
20–30 cm	42	150	40	41	44
30–40 cm	31	160	29	30	31
40–50 cm	22	133	20	20	22

[a]LF and HF represent low-density (< 1.6 g cm^{-3}) and high-density (> 1.6 g cm^{-3}) fractions, respectively.
[b]MAA and MIA represent macroaggregate (> 250 μm) and microaggregate (< 250 μm) fractions, respectively.
[c]NA: Not available.

In contrast to the density fractionation, the two MAA and MIA fractions obtained through the aggregate-size fractionation were very similar in the C content and its decreasing trend with soil depth. These fractions significantly differed in the size of soil aggregates, but seemed to consist of both organic and mineral materials at a similar percentage by mass in each of the soil layers at this forest site. In general, C content in soil aggregates increases with the size of aggregates because of a relatively large contribution of POM and fine roots in macroaggregate formation. However, a lack of aggregate size-dependent change in the C content has been reported for Andosols[59,73)].

SOC stocks in the density and aggregate-size fractions are summarized in **Table 8.3**. The density fractionation revealed that approximately 80% of the SOC was present in the HF fraction, i.e., in the form of organo-mineral associations. Only in the top 0–10 cm layer of the soil, the LF fraction represented a significant fraction to accumulate SOC. This is probably because of a continuous input of POM from the upper O layer through microbial decomposition of litter materials. The aggregate-size fractionation revealed that approximately two-thirds of the total SOC was present in association with

microaggregates. The result indicates that microaggregates play an important role in SOC accumulation in this soil. Note that the SOC stocks in the separated fractions (LF and HF fractions for the density fractionation, or MAA and MIA fractions for the aggregate-size fractionation) do not sum up to 100% in some soil layers due to a loss of SOC (mostly as dissolved organic carbon) during the fractionation procedure.

Table 8.3. SOC stocks (in kgC m^{-2}) in the density and aggregate-size fractions.

Layer	Density fractions[a]		Aggregate-size fractions[b]	
	LF	HF	MAA	MIA
0–10 cm	1.04 (24.2%)[c]	2.83 (65.7%)	0.98 (22.7%)	2.81 (65.3%)
10–20 cm	0.24 (8.8%)	2.29 (83.6%)	0.93 (34.0%)	1.56 (56.9%)
20–30 cm	0.16 (7.8%)	1.84 (90.2%)	0.74 (26.2%)	1.27 (62.3%)
30–40 cm	0.12 (8.5%)	1.33 (91.5%)	0.26 (17.8%)	1.17 (80.8%)
40–50 cm	0.10 (8.6%)	1.05 (91.4%)	0.23 (20.6%)	0.88 (78.0%)
Total	1.66 (14.2%)	9.34 (79.9%)	3.14 (26.9%)	7.69 (65.9%)

[a]LF and HF represent low-density (< 1.6 g cm^{-3}) and high-density (> 1.6 g cm^{-3}) fractions, respectively.
[b]MAA and MIA represent macroaggregate (> 250 μm) and microaggregate (< 250 μm) fractions, respectively.
[c]Number in parentheses indicates percentage of the total SOC stock in the soil layer.

8.5.2. Radiocarbon signatures of SOC

Conventional ^{14}C ages determined for the bulk soil, density fractions, and aggregate-size fractions are shown in **Table 8.4**. In general, ^{14}C age of SOC in the bulk soil increased with soil depth, ranging from Modern to more than 2000 years BP. This indicates that SOC in deeper soil layers is, on average, older than that in shallower soil layers. A question here is why the litter materials in the O horizon showed ^{14}C age of 50 years BP (or a negative $\Delta^{14}C$ value, also see **Table 8.5**); that is too old when considering that turnover times (as a result of the addition via litter fall and the decomposition) of litter materials are normally several years to a decade in O horizons of temperate forests[4,74]. A possible explanation for this is that the current atmospheric CO_2 in this region has a negative $\Delta^{14}C$ value with a contribution of CO_2 emission from ^{14}C-depleted fossil fuel combustion[75]. Thus the recently added litter materials in the O horizon might show an older ^{14}C age. To test this, we collected atmospheric samples at this site in 2018 and obtained $\Delta^{14}C$ values of around −16‰ for the atmospheric CO_2.

In contrast to the O horizon, SOC in the topmost 0–10 cm soil layer had a modern ^{14}C age, indicating a significant incorporation of ^{14}C-enriched organic materials that have been fixed since 1950 (i.e., the atmospheric nuclear weapons testing) in this soil layer. In the soil layers deeper than a depth of 10 cm, however, SOC was found to have resided in the soil long enough (several hundred to several thousand

years) for significant radioactive decay to occur.

Table 8.4. Conventional ^{14}C ages (in years BP) of the bulk soil, density fractions, and aggregate-size fractions.

Layer	Bulk	Density fractions[a]		Aggregate-size fractions[b]	
		LF	HF	MAA	MIA
O (litter)	50[c]	NA[e]	NA	NA	NA
0–10 cm	Modern[d]	Modern	Modern	Modern	Modern
10–20 cm	210	Modern	160	140	80
20–30 cm	1010	70	1000	1070	910
30–40 cm	1740	—[f]	1630	1740	1530
40–50 cm	2330	—	2400	2490	2230

[a]LF and HF represent low-density (< 1.6 g cm^{-3}) and high-density (> 1.6 g cm^{-3}) fractions, respectively.
[b]MAA and MIA represent macroaggregate (> 250 μm) and microaggregate (< 250 μm) fractions, respectively.
[c]The analytical uncertainty of the ^{14}C age was less than ± 50 years BP.
[d]Modern indicates that C in the sample contains post-1950, bomb-^{14}C.
[e]NA: Not available.
[f]The amount of sample obtained is small and not enough for ^{14}C analysis.

Soil organic carbon in the LF and HF fractions differed in ^{14}C age (**Table 8.4**). The SOC in the HF fraction, which is the predominant pool of C in this soil (see **Table 8.3**), had a ^{14}C age similar to that in the bulk soil, whereas the SOC in the LF fraction was significantly younger compared with the HF fraction (and the bulk soil). This result indicates that the SOC in the LF fraction represents a rapidly cycling pool of C in the soil. It is particularly interesting to see the stark contrast in ^{14}C age of SOC between the two fractions in the 20–30 cm soil layer. In contrast, SOC in the MAA and MIA fractions was relatively similar in ^{14}C age throughout the soil profile, although SOC in the MAA fraction was consistently older than that in the MIA fraction. This result suggests that, in general, SOC in soil aggregates with different size classes can turn over on a similar timescale in the same depth of this soil.

The $\Delta^{14}C$ values determined for the bulk soil, density fractions, and aggregate-size fractions are shown in **Table 8.5**. The $\Delta^{14}C$ values of SOC can be interpreted, however, as for the ^{14}C age: the $\Delta^{14}C$ value of SOC in the bulk soil decreased with soil depth, reflecting more contribution of bomb-^{14}C in the upper soil layers and more influence of ^{14}C radioactive decay in the deeper soil layers. The SOC in the LF fraction are enriched in ^{14}C (bomb-^{14}C) and therefore dominated by SOC fixed since 1950s. On the other hand, the SOC in the HF fraction generally consists of SOC fixed prior to 1950s. Two aggregate-size fractions show a similar $\Delta^{14}C$ value, indicating that cycling of SOC in these fractions, on average, occurs on a similar timescale.

Table 8.5. Radiocarbon signatures ($\Delta^{14}C$ in ‰) of the bulk soil, density fractions, and aggregate-size fractions.

Layer	Bulk	Density fractions[a]		Aggregate-size fractions[b]	
		LF	HF	MAA	MIA
O (litter)	−6.1[c]	NA[d]	NA	NA	NA
0–10 cm	35.9	64.7	50.8	63.3	62.0
10–20 cm	−25.6	78.0	−19.5	−17.7	−10.5
20–30 cm	−117.6	−8.4	−116.9	−124.3	−107.4
30–40 cm	−194.5	—	−183.8	−194.5	−173.0
40–50 cm	−251.4	—	−258.4	−266.1	−242.1

[a]LF and HF represent low-density (< 1.6 g cm^{-3}) and high-density (> 1.6 g cm^{-3}) fractions, respectively.
[b]MAA and MIA represent macroaggregate (> 250 μm) and microaggregate (< 250 μm) fractions, respectively.
[c]The analytical uncertainty of the $\Delta^{14}C$ value was 4–6‰.
[d]NA: Not available.

The SOC fractions obtained through any of the fractionation methods are still a mixture of young and old SOC; it has recently been revealed that even in deeper soil layers, decadally cycling SOC (i.e., SOC generated via photosynthesis since the atmospheric nuclear weapons testing and thus enriched in ^{14}C due to the incorporation of bomb-^{14}C) can exist[25]. This contradicts the assumption in the ^{14}C dating method that there has been no addition of ^{14}C in SOC in the soil sample since the SOC was added into the soil. In this respect, conventional ^{14}C age cannot represent real dynamics of SOC in many cases, particularly for SOC pools with a relatively young ^{14}C age (or a less ^{14}C-depleted $\Delta^{14}C$ value). For such semi-open systems like SOC, it should therefore be considered better to estimate its turnover time or mean residence time by considering both the inflow (addition of SOC via various soil processes) and outflow (loss of SOC via microbial decomposition (and radioactive decay for ^{14}C)) of C in a SOC pool. To achieve this, some modeling approaches have been proposed[4,23,25,45,55,76]. Details of these approaches are well explained and summarized in a chapter of the recently published book[65]. One thing we should note here is that these modeling approaches are all still built upon several assumptions.

As an example, a time-dependent single-pool model can be used to predict the change in $\Delta^{14}C$ value in a SOC pool:

$$F(t) = \{I(t-1) \cdot F_{atm}(t-1) + F(t-1) \cdot C(t-1) \cdot (1-k-\lambda)\} / C(t) \quad \text{(Eq. 8.1)}$$

where $F(t)$ represents the Fraction Modern of carbon (= $\Delta^{14}C(t)/1000+1$) in the SOC pool at year t, $I(t-1)$ the amount of C inputs to the SOC pool at year $t-1$ (i.e., in the previous 1-year time step), $F_{atm}(t-1)$ the Fraction Modern of carbon in the atmospheric CO_2 at year $t-1$, and $F(t-1)$ the Fraction Modern of carbon in the SOC at year at year $t-1$. $C(t)$ and $C(t-1)$ represent the amounts of C in the SOC

pool at years t and $t-1$, respectively, k represents the decomposition rate constant for the SOC pool (in y^{-1}), and λ the radioactive decay constant for ^{14}C (1.21×10^{-4} y^{-1}). $F_{atm}(t)$ is derived from the atmospheric ^{14}C-CO_2 record[22,77]. For the target SOC pool, we can predict $\Delta^{14}C$ value by using this model to find a value of k to the best explain the measured $\Delta^{14}C$ value, and then estimate the turnover time of the SOC pool as k^{-1} (in year)[25].

With the use of this modeling approach (Eq. 8.1), the turnover time of SOC for the O horizon (litter materials) can be estimated as 6 years based on its $\Delta^{14}C$ value (−6.1‰). The $\Delta^{14}C$ value (+35.9‰) of SOC in the topmost (0–10 cm) soil layer, which shows a contribution of bomb-^{14}C, yields two possible estimates for turnover time: approximately 11 and 190 years. The turnover times of SOC for the deeper soil layers can be estimated as approximately 450, 1190, 2020, and 2770 years for the 10–20 cm, 20–30 cm, 30–40 cm, and 40–50 cm soil layers, respectively.

8.5.3. Stable carbon and nitrogen isotope ratios of SOC

Stable carbon isotope ratios ($\delta^{13}C$) of the bulk soil, density fractions, and aggregate-size fractions are shown in **Table 8.6**. The $\delta^{13}C$ values of the O horizon was around −29‰, which was similar to $\delta^{13}C$ values of C3 plants, the current vegetation at this forest site. The $\delta^{13}C$ value of the bulk soil increased with soil depth. The $\delta^{13}C$ value of SOC is influenced by the degree of biological transformation and the vegetation (i.e., around −29‰ for C3 plants and around −13‰ for C4 plants)[78]. Regarding the effect of biological transformation, it is well documented that an enrichment of heavier isotopes (^{13}C) relative to lighter isotopes (^{12}C) in SOC occurs during its decomposition via biological metabolic processes of soil microorganisms[79,80]. Therefore, an increase in $\delta^{13}C$ value of SOC with depth can occur because SOC in deeper soil layers is more biologically transformed through repeated microbial processing. However, the ^{13}C enrichment through the biological transformation is typically within several per mil from the surface to deeper soil layers[80–82]. Therefore, the large change in the $\delta^{13}C$ value of SOC with depth (from −26.1‰ to −19.5‰) at this forest soil can be mostly attributed to change in the vegetation. The high $\delta^{13}C$ values (−19.5‰) observed for the deeper soil layers indicate an accumulation of SOC that originated from C4 plants, and suggest that the forest site was previously dominated by C4 plants and the vegetation had changed to current C3 plants.

For this study site, the amount of SOC of the previous C4-plant (grassland) origin in a soil can be estimated through a mass balance equation:

$$SOC_{C4} = (\delta^{13}C_{SOC} - \delta^{13}C_{C3}) / (\delta^{13}C_{C4} - \delta^{13}C_{C3}) \quad \text{(Eq. 8.2)}$$

where SOC_{C4} is the proportion of C4 plant-derived SOC (%), $\delta^{13}C_{SOC}$ is the $\delta^{13}C$ value of the SOC (‰), $\delta^{13}C_{C3}$ is the $\delta^{13}C$ value of C3 plant-derived SOC (‰), and $\delta^{13}C_{C4}$ is the $\delta^{13}C$ value of C4 plant-derived

SOC (‰), respectively. For instance, the contribution of the previous grassland-derived SOC to the SOC currently accumulated in the 40–50 cm soil layer can be estimated to be 59% by using the equation (Eq. 8.2) and the measured $\delta^{13}C$ values (i.e., $\delta^{13}C_{SOC}$ and $\delta^{13}C_{C3}$), when the value of $\delta^{13}C_{C4}$ is assumed to be −13‰[78]. Similarly, the contribution of grassland-derived SOC can be estimated as 18% of the total SOC in the 0–10 cm soil layer, which indicates that SOC in this layer is mostly of forest origin. This finding from $\delta^{13}C$ data is qualitatively consistent with ^{14}C results showing older SOC in deeper soil layers (**Tables 8.4 and 8.5**). In this way, using the ^{13}C data, we may be able to separate soil C into two different SOC pools with different origins (i.e., turnover times) without any physical and chemical fractionations of soil samples, if the study site had experienced a land use conversion (e.g., grassland to forest and forest to agricultural land) and information about when the conversion occurred can be obtained[83].

Table 8.6. Stable carbon isotope ratios ($\delta^{13}C$ in ‰) of the bulk soil, density fractions, and aggregate-size fractions.

Layer	Bulk	Density fractions[a]		Aggregate-size fractions[b]	
		LF	HF	MAA	MIA
O (litter)	−28.8	NA[c]	NA	NA	NA
0–10 cm	−26.1	−27.7	−25.2	−26.1	−25.4
10–20 cm	−22.9	−26.7	−22.7	−22.9	−22.9
20–30 cm	−20.3	−25.7	−20.2	−20.3	−20.3
30–40 cm	−19.5	−25.9	−19.4	−19.6	−19.5
40–50 cm	−19.5	−26.4	−19.4	−19.5	−19.4

[a]LF and HF represent low-density (< 1.6 g cm^{-3}) and high-density (> 1.6 g cm^{-3}) fractions, respectively.
[b]MAA and MIA represent macroaggregate (> 250 μm) and microaggregate (< 250 μm) fractions, respectively.
[c]NA: Not available.

The $\delta^{13}C$ values of the SOC fractions showed contrasting patterns between the two fractionation methods (**Table 8.6**). In the density fractionation, the HF fractions were similar in the $\delta^{13}C$ value to the bulk soils, but the LF fractions were lower in the $\delta^{13}C$ value compared with the bulk soils and HF fractions. This indicates that the SOC in the LF and HF fractions largely differ in its origin; the LF fractions consist mostly of SOC of the recent forest origin throughout the soil profile, whereas the HF fractions are a mixture of previous grassland- and recent forest-derived SOC with a depth trend in the mixture ratio. In contrast, in the aggregate-size fractionation, the $\delta^{13}C$ values of SOC were generally similar between the MAA and MIA fractions, indicating that both aggregate-size fractions have a similar mixture ratio of the grassland- and forest-derived SOC throughout the soil profile. These results are consistent with the results of ^{14}C analysis showing that the SOC in the LF fraction is younger than that in the HF fraction, and that the MAA and MIA fractions are generally similar in ^{14}C age or $\Delta^{14}C$

value in each of the soil layers (**Tables 8.4 and 8.5**).

It has been documented that, as with ^{13}C, ^{15}N is also enriched relative to ^{14}N during microbial decomposition of SOC[84]. Because $\delta^{15}N$ value is less affected by the vegetation, $\delta^{15}N$ value may be a better indicator of the degree of biological transformation of SOC in soils. Clear trends of increasing $\delta^{15}N$ value with soil depth were observed for the bulk soil and for the three SOC fractions (except the LF fraction) (**Table 8.7**), indicating that SOC in these soil and fractions is transformed more in deeper soil layers through microbial degradation. Consistent with the ^{14}C signatures, the $\delta^{15}N$ values suggest a relatively less degradation of SOC in the LF fractions, compared with the other fractions, throughout the soil profile. The concomitant increase in the $\delta^{15}N$ value and ^{14}C age with soil depth implies that the longer SOC resides in soil, the higher the degree of microbial transformation[85].

Table 8.7. Stable nitrogen isotope ratios ($\delta^{15}N$ in ‰) of the bulk soil, density fractions, and aggregate-size fractions.

Layer	Bulk	Density fractions[a]		Aggregate-size fractions[b]	
		LF	HF	MAA	MIA
O (litter)	−1.2	NA	NA	NA	NA
0–10 cm	2.4	0.0	3.5	2.2	3.2
10–20 cm	7.0	2.1	7.4	7.1	7.1
20–30 cm	9.6	3.2	10.0	9.8	9.8
30–40 cm	10.4	5.2.	10.1	10.6	10.7
40–50 cm	10.0	4.5	10.3	10.7	10.5

[a]LF and HF represent low-density (< 1.6 g cm^{-3}) and high-density (> 1.6 g cm^{-3}) fractions, respectively.
[b]MAA and MIA represent macroaggregate (> 250 μm) and microaggregate (< 250 μm) fractions, respectively.
[c]NA: Not available.

8.6. Summary

In this way, ^{14}C and stable isotope analyses are useful to understand and further quantify the carbon dynamics in soils. The isotope-based approaches enable us to compare the soil carbon dynamics in different terrestrial ecosystems and regions, which may offer a way to explore the diverse ecological roles of soils in the global carbon cycle. Studies using coupled carbon cycle–climate models suggest that soil carbon feedback to climate change could lead to a doubling of the projected warming by the end of this century. However, there is still a great deal of mechanistic uncertainty that underlies simulations of the responses of SOC to climate change. In these models, soils are generally characterized by several pools of SOC with specific turnover times. Therefore, quantification of SOC dynamics by using the ^{14}C approach can be incorporated into the models to improve their accuracy and

reliability. In addition, isotope-based approaches provide a unique opportunity to investigate how soil carbon dynamics changes along with, for example, land-use conversion and the progression of climate changes. Such investigations will be important to assess the impacts of natural and artificial processes on the global carbon cycle. Findings obtained through the isotope-based approaches are essential to improve our predictions of the future change in the Earth's climate.

Acknowledgements

This guide was prepared in collaboration between four Japanese organizations: Japan Atomic Energy Agency (JAEA), National Institute for Environmental Studies (NIES), The University of Tokyo, and Ibaraki University, through the project “Research on Climate Change using Nuclear and Isotopic Techniques” organized by the Ministry of Education, Culture, Sports, Science and Technology, Japan (MEXT), under the framework of the Forum for Nuclear Cooperation in Asia (FNCA).

Two of the co-authors, Untung Sugiharto of Natioanl Nuclear Energy Agency of Indonesia (BATAN) and Chakrit Saengkorakot of Thailand Institute of Nuclear Technology (TINT), acknowledge the financial support provided by the Nuclear Researchers Exchange Program of MEXT, to participate in this project.

The authors thank Toshiya Yoshida of the JAEA, and Munemasa Teramoto and Hajime Tomimatsu of the NIES for support with the fieldwork; Misuzu Kaminaga, Kikuko Yoshigaki, Mariko Ota, and Taro Ishii of the JAEA for support with the laboratory work; the staff at the Aomori Research and Development Center and the Tono Geoscience Center of JAEA for the AMS-^{14}C measurements; and Hamza El-Asaad of the JAEA for proofreading this document.

References

1) IPCC, Climate Change 2001, The Scientific Basis, Contribution of Working Group I to the Third Assessment Report of the Intergovernmental Panel on Climate Change, Cambridge University Press, Cambridge, UK, 2001, 881p.
2) IPCC, Climate Change 2013, The Physical Science Basis, Working Group I Contribution to the Fifth Assessment Report of the Intergovernmental Panel on Climate Change, Cambridge University Press, Cambridge, UK, 2013, 1535p.
3) Trumbore, S., Carbon respired by terrestrial ecosystems—recent progress and challenges, Glob. Change Biol., 12, 2006, pp.141–153.
4) Koarashi, J., Atarashi-Andoh, M., Ishizuka, S., Miura, S., Saito, T., Hirai, K., Quantitative aspects of heterogeneity in soil organic matter dynamics in a cool-temperate Japanese beech forest: a radiocarbon-based approach, Glob. Change Biol., 15, 2009, pp.631–642.
5) Melillo, J. M., Steudler, P. A., Aber, J. D., Newkirk, K., Lux, H., Bowles, F. P., Catricala, C., Magill, A., Ahrens, T., Morrisseau, S., Soil warming and carbon-cycle feedbacks to the climate system, Science, 298, 2002, pp.2173–2176.
6) Davidson, E. A., Janssens, I. A., Temperature sensitivity of soil carbon decomposition and feedbacks to climate change, Nature, 440, 2006, pp.165–173.
7) Teramoto, M., Liang, N., Takagi, M., Zeng, J., Grace, J., Sustained acceleration of soil carbon decomposition observed in a 6-year warming experiment in a warm-temperate forest in southern Japan, Sci. Rep., 6, 2016, 35563.
8) Teramoto, M., Liang, N., Ishida, S., Zeng, J., Long-term stimulatory warming effect on soil heterotrophic respiration in a cool-temperate broad-leaved deciduous forest in northern Japan, J. Geophys. Res. Biogeosci., 123, 2018, pp.1161–1177.
9) Jenkinson, D. S., Adams, D. E., Wild, A., Model estimates of CO_2 emissions from soil in response to global warming, Nature, 351, 1991, pp.304–306.
10) Cox, P. M., Betts, R. A., Jones, C. D., Spall, S. A., Totterdell, I. J., Acceleration of global warming due to carbon-cycle feedbacks in a coupled climate model, Nature, 408, 2000, pp.184–187.
11) Davidson, E. A., Belk, E., Boone, R. D., Soil water content and temperature as independent or confounded factors controlling soil respiration in a temperate mixed hardwood forest, Glob. Change Biol., 4, 1998, pp.217–227.
12) Lee, M., Nakane, K., Nakatsubo, T., Mo, W., Koizumi, H., Effects of rainfall events on soil CO_2 flux in a cool temperate deciduous broad-leaved forest, Ecol. Res., 17, 2002, pp.401–409.

13) Endo, N., Matsumoto, J., Yamamoto, N., Fukushima, A., Akasaka, I., Recent changes of precipitation amount and its characteristics in the world, J. Geol. (Chigaku Zasshi), 116, 2007, pp.824–835 (in Japanese with English abstract).
14) Fierer, N., Schimel, J. P., A proposed mechanism for the pulse in carbon dioxide production commonly observed following the rapid rewetting of a dry soil, Soil Sci. Soc. Am. J., 67, 2003, pp.798–805.
15) Xiang, S. R., Doyle, A., Holden, P. A., Schimel, J. P., Drying and rewetting effects on C and N mineralization and microbial activity in surface and subsurface California grassland soils, Soil Biol. Biochem., 40, 2008, pp.2281–2289.
16) Nagano, H., Atarashi-Andoh, M., Koarashi, J., Effect of dry-wet cycles on carbon dioxide release from two volcanic ash soils in a Japanese temperate forest, Soil Sci. Plant Nutr., 65, 2019, pp.525–533.
17) Wei, X., Shao, M., Gale, W., Li, L., Global pattern of soil carbon losses due to the conversion of forests to agricultural land, Sci. Rep., 4, 2014, 4062.
18) Ball, T., Smith, K. A., Garnett, M. H., Moncrieff, J. B., Zerva, A., An assessment of the effect of Sitka Spruce (Picea sitchensis Bong. Carr) plantation forest cover on carbon turnover and torage in a peaty glaey soil, Eur. J. Soil Sci., 62, 2011, pp.560–571.
19) Lal, R., Kimble, J. M., Conservation tillage for carbon sequestration, Nutr. Cycl. Agroecosys., 49, 1997, pp.243–253.
20) Trumbore, S., Age of soil organic matter and soil respiration: Radiocarbon constraints on belowground dynamics, Ecol. Applic., 10, 2000, pp.399–411.
21) Schuur, E. A. G., Carbone, M. S., Hicks Pries, C. E., Hopkins, F. M., Natali, S. M., Radiocarbon in Terrestrial Systems, In: Radiocarbon and Climate Change (Eds. Schuur, E. A. G., Druffel, E. R. M., Trumbore, S. E), Springer, Switzerland, 2016, pp.167–220.
22) Hua, Q., Barbetti, M., Rokowski, A. Z., Atmospheric radiocarbon for the period 1950–2010, Radiocarbon, 55, 2013, pp.2059–2072.
23) Hsieh, Y. -P., Radiocarbon signatures of turnover rates in active soil organic carbon pools, Soil Sci. Soc. Am. J., 57, 1993, pp.1020–1022.
24) Hahn, V., Hogberg, P., Buchmann, N., ^{14}C – a tool for separation of autotrophic and heterotrophic soil respiration, Glob. Change Biol., 12, 2006, pp.972–982.
25) Koarashi, J., Hockaday, W. C., Masiello, C. A., Trumbore, S. E., Dynamics of decadally cycling carbon in subsurface soils, J. Geophys. Res., 117, 2012, G03033.
26) Atarashi-Andoh, M., Koarashi, J., Ishizuka, S., Hirai, K., Seasonal patterns and control factors of CO_2 effluxes from surface litter, soil organic carbon, and root-derived carbon estimated using radiocarbon signatures, Agric. For. Meteorol., 152, 2012, pp.149–158.

27) Hajdas, I., Applications of radiocarbon dating method, Radiocarbon, 51, 2009, pp.79–90.
28) Palincaş, N., Radiocarbon dating in archaeology: Interdisciplinary aspects and consequences (an overview), AIP Conference Proceedings, 1852, 2017, 060006.
29) Trumbore, S. E., Zheng, S., Comparison of fractionation methods for soil organic matter ^{14}C analysis, Radiocarbon, 38, 1996, pp.219–229.
30) von Lützow, M., Kögel-Knabner, I., Ekschmitt, K., Flessa, H., Guggenberger, G., Matzner, E., Marschner, B., SOM fractionation methods: Relevance to functional pools and to stabilization mechanisms, Soil Biol. Biochem., 39, 2007, pp.2183–2207.
31) Castanha, C., Trumbore, S., Amundson, R., Methods of separating soil carbon pools affect the chemistry and turnover of isolated fractions, Radiocarbon, 50, 2008, pp.83–97.
32) Koarashi, J., Atarashi-Andoh, M., Amano, H., Matsunaga, T., Vertical distributions of global fallout ^{137}Cs and ^{14}C in a Japanese forest soil profile and their implications for the fate and migration processes of Fukushima-derived ^{137}Cs, J. Radioanal. Nucl. Chem., 311, 2017, pp.473–481.
33) Koarashi, J., Atarashi-Andoh, M., Matsunaga, T., Sato, T., Nagao, S., Nagai, H., Factors affecting vertical distribution of Fukushima accident-derived radiocesium in soil under different land-use conditions, Sci. Total Environ., 431, 2012, pp.392–401.
34) Nakanishi, T., Atarashi-Andoh, M., Koarashi, J., Saito-Kokubu, Y., Hirai, K., Carbon isotopes of water-extractable organic carbon in a depth profile of forest soil imply a dynamic relationship with soil carbon, Eur. J. Soil Sci., 63, 2012, pp.495–500.
35) Canadian Society of Soil Science, Soil Sampling and Methods of Analysis, Second Edition (Eds. Carter, M. R. and Gregorich, E. G.), CRC Press, FL, USA, 2007, 1262p.
36) Soil Survey Staff, Kellogg Soil Survey Laboratory Methods Manual, Soil Survey Investigations Reports No. 42, Version 5.0 (Eds. Burt, R. and Soil Survey Staff), United States Department of Agriculture, Natural Resources Conservation Service, Washington DC, USA, 2014.
37) Soil Science Society of America, Methods of Soil Analysis: Part 1 Physical and Mineralogical Methods, 5.1, Second Edition (Ed. Klute, A.), American Society of Agronomy, Inc. and Soil Science Society of America, Inc., Madison, Wisconsin, USA, 1986, 1188p.
38) Soil Science Society of America, Methods of Soil Analysis: Part 2 Chemical and Microbiological Properties, 9.2.2, Second Edition (Ed. Page, A. L.), American Society of Agronomy, Inc. and Soil Science Society of America, Inc., Madison, Wisconsin, USA, 1982, 1159p.
39) Soil Science Society of America, Methods of Soil Analysis: Part 3 Chemical Methods (Eds. Sparks, D. L., Page, A. L., Helmke, P. A., Loeppert R. H., Soltanpour, P. N., Tabatabai, M. A.,

Johnston. C. T., Sumner, M. E.), Soil Science Society of America, Inc. and American Society of Agronomy, Inc., Madison, Wisconsin, USA, 1996, 1390p.

40) Soil Science Society of America, Methods of Soil Analysis: Part 4 Physical Methods (Eds. Dane, J. H., Clarke Topp, G.), Soil Science Society of America, Inc., Madison, Wisconsin, USA, 2002, 1692p.
41) Soil Science Society of America, Methods of Soil Analysis: Part 5 Mineralogical Methods (Eds. Ulery, A. L., Drees, L. R.), Soil Science Society of America, Inc., Madison, Wisconsin, USA, 2008, 521p.
42) Muto, K., Atarashi-Andoh, M., Matsunaga, T., Koarashi, J., Characterizing vertical migration of ^{137}Cs in organic layer and mineral soil in Japanese forests: Four-year observation and model analysis, J. Environ. Radioact., 208–209, 2019, 106040.
43) Schnitzer, M., Soil organic matter – the next 75 years, Soil Sci., 151, 1991, pp.41–58.
44) von Lützow, M., Kögel-Knabner, I., Ekschmitt, K., Matzner, E., Guggenberger, G., Marschner, B., Flessa, H., Stabilization of organic matter in temperate soils: mechanisms and their relevance under different soil conditions – a review, Eur. J. Soil Sci., 57, 2006, pp.426–445.
45) Trumbore S. E., Chadwick, O. A., Amundson, R., Rapid exchange between soil carbon and atmospheric carbon dioxide driven by temperature change, Science, 272, 1996, pp.393–396.
46) Christensen, B. T., Physical fractionation of soil and structural and functional complexity in organic matter turnover, Eur. J. Soil Sci., 52, 2001, pp.345–353.
47) Sollins, P., Swanston, C., Kleber, M., Filley, T., Kramer, M., Crow, S., Caldwell, B. A., Lajtha, K., Bowden, R., Organic C and N stabilization in a forest soil: Evidence from sequential density fractionation, Soil Biol. Biochem., 38, 2006, pp.3313–3324.
48) Wagai, R., Mayer, L. M., Kitayama, K., Nature of the “occluded” low-density fraction in soil organic matter studies: A critical review, Soil Sci. Plant Nutr., 55, 2009, pp.13–25.
49) Koarashi, J., Nishimura, S., Atarashi-Andoh, M., Matsunaga, T., Sato, T., Nagao, S., Radiocesium distribution in aggregate-size fractions of cropland and forest soils affected by the Fukushima nuclear accident, Chemosphere, 205, 2018, pp.147–155.
50) Koarashi, J., Nishimura, S., Atarashi-Andoh, M., Muto, K., Matsunaga, T., A new perspective on the ^{137}Cs retention mechanism in surface soils during the early stage after the Fukushima nuclear accident, Sci. Rep., 9, 2019, 7034.
51) Paul, E. A., Follett, R. F., Leavitt, S. W., Halvorson, A., Peterson, G. A., Lyon, D. J., Radiocarbon dating for determination of soil organic matter pool sizes and dynamics, Soil Sci. Soc. Am. J., 61, 1997, pp.1058–1067.
52) Eusterhues, K., Rumpel, C., Kögel-Knabner, I., Stabilization of soil organic matter isolated via oxidative degradation, Org. Geochem., 36, 2005, pp.1567–1575.

53) Jagadamma, S., Lal, R., Ussiri, D. A. N., Trumbore, S. E., Mestelan, S., Evaluation of structural chemistry and isotopic signatures of refractory soil organic carbon fraction isolated by wet oxidation methods, Biogeochem., 98, 2010, pp.29–44.

54) Marzaioli, F., Lubritto, C., Del Galdo, I., D'Onofrio, A., Cotrufo, M. F., Comparison of different soil organic matter fractionation methodologies: Evidences from ultrasensitive ^{14}C measurements, Nucl. Instr. Meth. Phys. Res. Sect. B, 268, 2010, pp.1062–1066.

55) Baisden, W. T., Amundson, R., Cook, A. C., Brenner, D. L., Turnover and storage of C and N in five density fractions from California annual grassland surface soils, Glob. Biogeochem. Cyc., 16, 2002, 1117.

56) Crow, S. E., Swanston, C. W., Lajtha, K., Brooks, J. R., Keirstead, H., Density fractionation of forest soils: Methodological questions and interpretation of incubation results and turnover time in an ecosystem context, Biogeochem., 85, 2007, pp.69–90.

57) Tisdall, J. M., Oades, J. M., Organic matter and water-stable aggregates in soils, Eur. J. Soil Sci., 33, 1982, pp.141–163.

58) Six, J., Bossuyt, H., Degryze, S., Denef, K., A history of research on the link between (macro)aggregates, soil biota, and soil organic matter dynamics, Soil Till. Res., 79, 2004, pp.7–31.

59) Asano, M., Wagai, R., Evidence of aggregate hierarchy at micro- to submicron scales in an allophanic Andisol, Geoderma, 216, 2014, pp.62–74.

60) Aramaki, T., Mizushima, T., Mizutani, Y., Yamamoto, T., Togawa, O., Kabuto, S., Kuji, T., Gottdang, A., Klein, M., Mous, D. J. W., The AMS facility at the Japan Atomic Energy Research Institute (JAERI), Nucl. Instr. Meth. Phys. Res. Sect. B, 172, 2000, pp.18–23.

61) Xu, X., Trumbore, S. E., Zheng, S., Southon, J. R., McDuffee. K. E., Luttgen, M., Liu, J. C., Modifying a sealed tube zinc reduction method for preparation of AMS graphite targets: Reducing background and attaining high precision, Nucl. Instr. Meth. Phys. Res. Sect. B, 259, 2007, pp.320–329.

62) Trumbore, S. E., Xu, X., Santos, G. M., Czimczik, C. I., Beaupré, S. R., Pack, M. A., Hopkins, F. M., Stills, A., Lupascu, M., Ziolkowski, L., Preparation for Radiocarbon Analysis, In: Radiocarbon and Climate Change (Eds. Schuur, E. A. G., Druffel, E. R. M., Trumbore, S. E), Springer, Switzerland, 2016, pp.279–315.

63) Wacker, L., Němec, M., Bourquin, J., A revolutionary graphitisation system: Fully automated, compact and simple, Nucl. Instr. Meth. Phys. Res. Sect. B, 268, 2010, pp.931–934.

64) Saito-Kokubu, Y., Fujita, N., Miyake, M., Watanabe, T., Ishizaka, C., Okabe, N., Ishimaru, T., Matsubara, A., Nishizawa, A., Nishio, T., Kato, M., Torazawa, H., Isozaki, N., Current status

of JAEA-AMS-TONO in the 20th year, Nucl. Instr. Meth. Phys. Res. Sect. B, 456, 2019, pp.217–275.

65) Trumbore, S. E., Sierra, C. A., Hicks Pries, C. E., Radiocarbon Nomenclature, Theory, Models, and Interpretation: Measuring Age, Determining Cycling Rates, and Tracing Source Pools, In: Radiocarbon and Climate Change (Eds. Schuur, E. A. G., Druffel, E. R. M., Trumbore, S. E), Springer, Switzerland, 2016, pp.45–82.

66) Saito-Kokubu, Y., Matsubara, A., Miyake, M., Nishizawa, A., Ohwaki, Y., Nishio, T., Sanada, K., Hanaki, T., Progress on multi-nuclide AMS of JAEA-AMS-TONO, Nucl. Instr. Meth. Phys. Res. Sect. B, 361, 2015, pp.48–53.

67) Maden, C., Anastasi, P. A. F., Dougans, A., Freeman, S. P. H. T., Kitchen, R., Klody, G., Schnabel, C., Sundquist, M., Vanner, K., Xu, S., SUERC AMS ion detection, Nucl. Instr. Meth. Phys. Res. Sect. B, 259, 2007, pp.131–139.

68) Matsuzaki, H., Nakano, C., Tsuchiya, Y. S., Ito, S., Morita, A., Kusuno, H., Miyake, Y., Honda, M., Bautista VII, A. T., Kawamoto, M., Tokuyama, H., The status of the AMS system at MALT in its 20th year, Nucl. Instr. Meth. Phys. Res. Sect. B, 361, 2015, pp.63–68.

69) Matsuzaki, H., Miyake, Y., Nakashoji, K., Tokuyama, H., Sunohara Tsuchiya, Y., Kusuno, H., Toya, M., Current status of MALT AMS facility: A report of updated performance and recent achievement, Nucl. Instr. Meth. Phys. Res. Sect. B, 463, 2020, pp.55–63.

70) Stuiver, M., Polach, H. A., Discussion: Reporting of ^{14}C data, Radiocarbon, 19, 1977, pp.355–363.

71) Jobbágy, E. G., Jackson, R. B., The vertical distribution of soil organic carbon and its relation to climate and vegetation, Ecol. Applic., 10, 2000, pp.423–436.

72) Nanzyo, M., Dahlgren, R., Shoji, S., Chemical characteristics of volcanic ash soils, In: Volcanic Ash Soils: Genesis, Properties and Utilization (Eds. Shoji, S., Nanzyo, M., Dahlgren, R.), Elsevier, The Netherlands, 1993, pp.145–187

73) Huygens, D., Boeckx, P., Van Cleemput, O., Oyarzún, C., Godoy, R., Aggregate and soil organic carbon dynamics in South Chilean Andisols, Biogeosci., 2, 2005, pp.159–174.

74) Ono, K., Hiradate, S., Morita, S., Hirai, K., Fate of organic carbon during decomposition of different litter types in Japan, Biogeochem., 112, 2013, pp.7–21.

75) Rokowski, A. Z., Nakamura, T., Pazdur, A., Variations of anthropogenic CO_2 in urban area deduced by radiocarbon concentration in modern tree tings, J. Environ. Radioact., 99, 2008, pp.1558–1565.

76) Torn, M. S., Swanston, C. W., Castanha, C., Trumbore, S. E., Storage and turnover of natural organic matter in soil, In: Biophysico-Chemical Processes Involving Natural Nonliving

Organic Matter in Environmental Systems, IUPAC Ser. Biophysico-chem. Processes Environ. Syst., vol. 2 (Eds. Hunag, P. M., Senesi. N.), John Wiley & Sons., 2009, pp.219–272.

77) Levin, I., Kromer, B., The tropospheric $^{14}CO_2$ level in mid-latitudes of the northern hemisphere (1959–2003), Radiocarbon, 48, 2004, pp.1261–1272.

78) Cerling, T. E., Harris, J. M., Carbon isotope fractionation between diet and bioapatite in ungulate mammals and implications for ecological and paleoecological studies, Oecologia, 120, 1999, pp.347–363.

79) Wedin, D. A., Tieszen, L. L., Dewey, B., Pastor, J., Carbon isotope dynamics during grass decomposition and soil organic matter formation, Ecology, 76, 1995, pp.1383–1392.

80) Wijesinghe, J. N., Koarashi, J., Atarashi-Andoh, M., Saito-Kokubu, Y., Yamaguchi, N., Sase, T., Hosono, M., Inoue, Y., Mori, Y., Hiradate, S., Formation and mobility of soil organic carbon in a buried humic horizon of a volcanic ash soil, Geoderma, 374, 2020, 114417.

81) Accoe, F., Boeckx, P., Van Cleemput, O., Hofman, G., Relationship between soil organic C degradability and the evolution of the $\delta^{13}C$ signature in profiles under permanent grassland, Rapid Commun. Mass Spectrom., 17, 2003, pp.2591–2596.

82) Wynn, J. G., Bird, M. I., Wong, N. L., Rayleigh distillation and the depth profile of $^{13}C/^{12}C$ ratios of soil organic carbon from soils of disparate texture in Iron Range National Park, Far North Queensland, Australia, Geochim. Cosmochim. Acta, 69, 2005, pp.1961–1973.

83) Balesdent, J., Basile-Doelsch, I., Chadoeuf, J., Cornu, S., Derrien, D., Fekiacova, Z., Hatté, C., Atmosphere–soil carbon transfer as a function of soil depth, Nature, 559, 2018, pp.599–602.

84) Craine, J. M., Brookshire, E. N. J., Cramer. M. D., Hasselquist, N. J., Koba, K., Marion-Spiotta, E., Wang, L., Ecological interpretations of nitrogen isotope ratios of terrestrial plants and soils, Plant Soil, 396, 2015, pp.1–26.

85) Meyer, S., Leifeld, J., Concurrent increase in ^{15}N and radiocarbon age in soil density fractions, J. Plant Nutr. Soil Sci., 176, 2013, pp.505–508.

This is a blank page.

国際単位系（SI）

表１．SI 基本単位

基本量	SI 基本単位	
	名称	記号
長さ	メートル	m
質量	キログラム	kg
時間	秒	s
電流	アンペア	A
熱力学温度	ケルビン	K
物質量	モル	mol
光度	カンデラ	cd

表２．基本単位を用いて表されるSI組立単位の例

組立量	SI 組立単位	
	名称	記号
面積	平方メートル	m^2
体積	立方メートル	m^3
速さ，速度	メートル毎秒	m/s
加速度	メートル毎秒毎秒	m/s^2
波数	毎メートル	m^{-1}
密度，質量密度	キログラム毎立方メートル	kg/m^3
面積密度	キログラム毎平方メートル	kg/m^2
比体積	立方メートル毎キログラム	m^3/kg
電流密度	アンペア毎平方メートル	A/m^2
磁界の強さ	アンペア毎メートル	A/m
量濃度(a)，濃度	モル毎立方メートル	mol/m^3
質量濃度	キログラム毎立方メートル	kg/m^3
輝度	カンデラ毎平方メートル	cd/m^2
屈折率(b)	（数字の） 1	1
比透磁率(b)	（数字の） 1	1

(a) 量濃度（amount concentration）は臨床化学の分野では物質濃度（substance concentration）ともよばれる。
(b) これらは無次元量あるいは次元１をもつ量であるが、そのことを表す単位記号である数字の１は通常は表記しない。

表３．固有の名称と記号で表されるSI組立単位

組立量	SI 組立単位			
	名称	記号	他のSI単位による表し方	SI基本単位による表し方
平面角	ラジアン(b)	rad	1 (b)	m/m
立体角	ステラジアン(b)	sr(c)	1 (b)	m^2/m^2
周波数	ヘルツ(d)	Hz		s^{-1}
力	ニュートン	N		$m\ kg\ s^{-2}$
圧力，応力	パスカル	Pa	N/m^2	$m^{-1}\ kg\ s^{-2}$
エネルギー，仕事，熱量	ジュール	J	N m	$m^2\ kg\ s^{-2}$
仕事率，工率，放射束	ワット	W	J/s	$m^2\ kg\ s^{-3}$
電荷，電気量	クーロン	C		s A
電位差（電圧），起電力	ボルト	V	W/A	$m^2\ kg\ s^{-3}\ A^{-1}$
静電容量	ファラド	F	C/V	$m^{-2}\ kg^{-1}\ s^4\ A^2$
電気抵抗	オーム	Ω	V/A	$m^2\ kg\ s^{-3}\ A^{-2}$
コンダクタンス	ジーメンス	S	A/V	$m^{-2}\ kg^{-1}\ s^3\ A^2$
磁束	ウエーバ	Wb	Vs	$m^2\ kg\ s^{-2}\ A^{-1}$
磁束密度	テスラ	T	Wb/m^2	$kg\ s^{-2}\ A^{-1}$
インダクタンス	ヘンリー	H	Wb/A	$m^2\ kg\ s^{-2}\ A^{-2}$
セルシウス温度	セルシウス度(e)	℃		K
光束	ルーメン	lm	cd sr(c)	cd
照度	ルクス	lx	lm/m^2	m^{-2} cd
放射性核種の放射能(f)	ベクレル(d)	Bq		s^{-1}
吸収線量，比エネルギー分与，カーマ	グレイ	Gy	J/kg	$m^2\ s^{-2}$
線量当量，周辺線量当量，方向性線量当量，個人線量当量	シーベルト(g)	Sv	J/kg	$m^2\ s^{-2}$
酸素活性	カタール	kat		s^{-1} mol

(a)SI接頭語は固有の名称と記号を持つ組立単位と組み合わせても使用できる。しかし接頭語を付した単位はもはやコヒーレントではない。
(b)ラジアンとステラジアンは数字の１に対する単位の特別な名称で、量についての情報をつたえるために使われる。実際には、使用する時には記号radおよびsrが用いられるが、習慣として組立単位としての記号である数字の１は明示されない。
(c)測光学ではステラジアンという名称と記号srを単位の表し方の中に、そのまま維持している。
(d)ヘルツは周期現象についてのみ、ベクレルは放射性核種の統計的過程についてのみ使用される。
(e)セルシウス度はケルビンの特別な名称で、セルシウス温度を表すために使用される。セルシウス度とケルビンの単位の大きさは同一である。したがって、温度差や温度間隔を表す数値はどちらの単位で表しても同じである。
(f)放射性核種の放射能（activity referred to a radionuclide）は、しばしば誤った用語で"radioactivity"と記される。
(g)単位シーベルト（PV,2002,70,205）についてはCIPM勧告2（CI-2002）を参照。

表４．単位の中に固有の名称と記号を含むSI組立単位の例

組立量	SI 組立単位		
	名称	記号	SI 基本単位による表し方
粘度	パスカル秒	Pa s	$m^{-1}\ kg\ s^{-1}$
力のモーメント	ニュートンメートル	N m	$m^2\ kg\ s^{-2}$
表面張力	ニュートン毎メートル	N/m	$kg\ s^{-2}$
角速度	ラジアン毎秒	rad/s	$m\ m^{-1}\ s^{-1}=s^{-1}$
角加速度	ラジアン毎秒毎秒	rad/s^2	$m\ m^{-1}\ s^{-2}=s^{-2}$
熱流密度，放射照度	ワット毎平方メートル	W/m^2	$kg\ s^{-3}$
熱容量，エントロピー	ジュール毎ケルビン	J/K	$m^2\ kg\ s^{-2}\ K^{-1}$
比熱容量，比エントロピー	ジュール毎キログラム毎ケルビン	J/(kg K)	$m^2\ s^{-2}\ K^{-1}$
比エネルギー	ジュール毎キログラム	J/kg	$m^2\ s^{-2}$
熱伝導率	ワット毎メートル毎ケルビン	W/(m K)	$m\ kg\ s^{-3}\ K^{-1}$
体積エネルギー	ジュール毎立方メートル	J/m^3	$m^{-1}\ kg\ s^{-2}$
電界の強さ	ボルト毎メートル	V/m	$m\ kg\ s^{-3}\ A^{-1}$
電荷密度	クーロン毎立方メートル	C/m^3	m^{-3} s A
表面電荷	クーロン毎平方メートル	C/m^2	m^{-2} s A
電束密度，電気変位	クーロン毎平方メートル	C/m^2	m^{-2} s A
誘電率	ファラド毎メートル	F/m	$m^{-3}\ kg^{-1}\ s^4\ A^2$
透磁率	ヘンリー毎メートル	H/m	$m\ kg\ s^{-2}\ A^{-2}$
モルエネルギー	ジュール毎モル	J/mol	$m^2\ kg\ s^{-2}\ mol^{-1}$
モルエントロピー，モル熱容量	ジュール毎モル毎ケルビン	J/(mol K)	$m^2\ kg\ s^{-2}\ K^{-1}\ mol^{-1}$
照射線量（X線及びγ線）	クーロン毎キログラム	C/kg	kg^{-1} s A
吸収線量率	グレイ毎秒	Gy/s	$m^2\ s^{-3}$
放射強度	ワット毎ステラジアン	W/sr	$m^4\ m^{-2}\ kg\ s^{-3}=m^2\ kg\ s^{-3}$
放射輝度	ワット毎平方メートル毎ステラジアン	$W/(m^2\ sr)$	$m^2\ m^{-2}\ kg\ s^{-3}=kg\ s^{-3}$
酵素活性濃度	カタール毎立方メートル	kat/m^3	$m^{-3}\ s^{-1}$ mol

表５．SI 接頭語

乗数	名称	記号	乗数	名称	記号
10^{24}	ヨタ	Y	10^{-1}	デシ	d
10^{21}	ゼタ	Z	10^{-2}	センチ	c
10^{18}	エクサ	E	10^{-3}	ミリ	m
10^{15}	ペタ	P	10^{-6}	マイクロ	μ
10^{12}	テラ	T	10^{-9}	ナノ	n
10^9	ギガ	G	10^{-12}	ピコ	p
10^6	メガ	M	10^{-15}	フェムト	f
10^3	キロ	k	10^{-18}	アト	a
10^2	ヘクト	h	10^{-21}	ゼプト	z
10^1	デカ	da	10^{-24}	ヨクト	y

表６．SIに属さないが、SIと併用される単位

名称	記号	SI 単位による値
分	min	1 min=60 s
時	h	1 h =60 min=3600 s
日	d	1 d=24 h=86 400 s
度	°	1°=(π/180) rad
分	’	1’=(1/60)°=(π/10 800) rad
秒	”	1”=(1/60)’=(π/648 000) rad
ヘクタール	ha	1 ha=1 $hm^2=10^4m^2$
リットル	L, l	1 L=1 l=1 $dm^3=10^3cm^3=10^{-3}m^3$
トン	t	1 t=10^3 kg

表７．SIに属さないが、SIと併用される単位で、SI単位で表される数値が実験的に得られるもの

名称	記号	SI 単位で表される数値
電子ボルト	eV	1 eV=1.602 176 53(14)×10^{-19}J
ダルトン	Da	1 Da=1.660 538 86(28)×10^{-27}kg
統一原子質量単位	u	1 u=1 Da
天文単位	ua	1 ua=1.495 978 706 91(6)×10^{11}m

表８．SIに属さないが、SIと併用されるその他の単位

名称	記号	SI 単位で表される数値
バール	bar	1 bar=0.1MPa=100 kPa=10^5Pa
水銀柱ミリメートル	mmHg	1 mmHg≈133.322Pa
オングストローム	Å	1 Å=0.1nm=100pm=10^{-10}m
海里	M	1 M=1852m
バーン	b	1 b=100fm^2=$(10^{-12}cm)^2$=$10^{-28}m^2$
ノット	kn	1 kn=(1852/3600)m/s
ネーパ	Np	SI単位との数値的な関係は、対数量の定義に依存。
ベル	B	
デシベル	dB	

表９．固有の名称をもつCGS組立単位

名称	記号	SI 単位で表される数値
エルグ	erg	1 erg=10^{-7} J
ダイン	dyn	1 dyn=10^{-5}N
ポアズ	P	1 P=1 dyn s cm^{-2}=0.1Pa s
ストークス	St	1 St =1$cm^2\ s^{-1}$=$10^{-4}m^2\ s^{-1}$
スチルブ	sb	1 sb =1cd cm^{-2}=10^4cd m^{-2}
フォト	ph	1 ph=1cd sr cm^{-2} =10^4lx
ガル	Gal	1 Gal =1cm s^{-2}=$10^{-2}ms^{-2}$
マクスウエル	Mx	1 Mx = 1G cm^2=10^{-8}Wb
ガウス	G	1 G =1Mx cm^{-2} =10^{-4}T
エルステッド(a)	Oe	1 Oe ≙ $(10^3/4\pi)$A m^{-1}

(a) ３元系のCGS単位系とSIでは直接比較できないため、等号「 ≙ 」は対応関係を示すものである。

表10．SIに属さないその他の単位の例

名称	記号	SI 単位で表される数値
キュリー	Ci	1 Ci=3.7×10^{10}Bq
レントゲン	R	1 R = 2.58×10^{-4}C/kg
ラド	rad	1 rad=1cGy=10^{-2}Gy
レム	rem	1 rem=1 cSv=10^{-2}Sv
ガンマ	γ	1 γ=1 nT=10^{-9}T
フェルミ		1 フェルミ=1 fm=10^{-15}m
メートル系カラット		1 メートル系カラット= 0.2 g = 2×10^{-4}kg
トル	Torr	1 Torr = (101 325/760) Pa
標準大気圧	atm	1 atm = 101 325 Pa
カロリー	cal	1 cal=4.1858J（「15℃」カロリー），4.1868J（「IT」カロリー），4.184J（「熱化学」カロリー）
ミクロン	μ	1 μ =1μm=10^{-6}m

（第8版，2006年）